The
ENGINEERS' DIGEST

REVIEW OF ENGINEERING PROGRESS ABROAD

VOL. VI. No. 6 JUNE, 1945

AUG 2 3 1945
ENGINEERING LIBRARY

Churchill
PRECISION GRINDING MACHINES
GRINDING FROM THE SOLID ECCENTRIC FINS ON AERO ENGINE CYLINDERS USING A MULTI-RIBBED WHEEL
There is a CHURCHILL machine for every precision grinding job..
Machinery
THE CHURCHILL MACHINE TOOL CO., LTD., MANCHESTER.
HOME SELLING AGENTS . . . CHARLES CHURCHILL & CO. LTD. (BIRMINGHAM & BRANCHES)
EXPORT SALES ORGANISATION . . ASSOCIATED BRITISH MACHINE TOOL MAKERS Ltd. (London & Branches)

THE ENGINEERS' DIGEST

REVIEW OF ENGINEERING PROGRESS ABROAD

Published Monthly at 120, Wigmore Street, London, W. 1.

Publishers : **ENGINEERS' DIGEST LTD.** – – – – – – – Telephone : WELBECK 9357

Advertisement Dept. – 120, Wigmore Street, London, W.1. – – Telephone : WELBECK 9357

Distribution – – E. & F. N. SPON, LTD., 57, Haymarket, London, S.W.1.
Telephone : Whitehall 1860. Telegrams : Fenspon, Lesquare, London

Editorial Dept. – – 120, Wigmore Street, London, W.1. – – Telephone : WELBECK 9357

Subscriptions to : ENGINEERS' DIGEST LTD., 120, Wigmore Street, London, W.1, or
E. & F. N. SPON, LTD., 57, Haymarket, London, S.W.1.

ANNUAL SUBSCRIPTION OF 12 NUMBERS, £2 2s. SINGLE COPIES, 4s. 6d.

ADVISORY COMMITTEE

J. F. ALCOCK, B.A., A.M.I.Mech.E.
R. W. ALLOTT, M.A., A.R.Ae.S.
E. ALTON, D.Eng., A.M.Inst.B.E.
H. H. ASBRIDGE, M.B.E., M.I.Mech.E.
R. W. AYERS, M.I.W.
Col. J. BOWDEN, M.Inst.C.E., M.I.Mech.E.
H. H. BROUGHTON, M.I.Mech.E.
F. BUCKINGHAM, B.Sc., A.M.Inst.C.E., A.M.I.Mech.E.,
T. H. BURNHAM, B.Sc. (Lond.), A.M.I.Mech.E. [A.M.I.E.E.
J. S. CASWELL, M.Sc., M.I.Mech.E.
G. C. SAFFERY COOPER.
J. DICK, Ph.D., B.Sc., A.M.I.Mech.E.
D. FIFE, M.I.Mech.E.
G. E. FOXWELL, D.Sc. (Lond.), F.Inst.P., F.Inst.F.,
R. GRIFFITHS, M.Sc. [M.Inst.Gas.E.
H. HEYWOOD, Ph.D., M.Sc. (Eng.), A.M.I.Mech.E.
O. HURST, M.Inst.N.A.
Capt. J. S. IRVING, M.I.Mech.E., M.I.A.E., A.F.R.Ae.S., M.S.A.E.
F. C. JOHANSEN, M.Sc. (Eng.), M.I.Mech.E., F.R.Ae.S., M.I.Loco.E.
W. J. KEARTON, D.Eng., M.I.Mech.E., A.M.Inst.N.A.
Prof. W. KERR, Ph.D., M.I.Mech.E.
G. V. LOMONOSOFF, Dr.Ing., M.I.Mech.E.
B. J. LYMER, M.I.Mech.E.
D. T. MacIVOR, M.I.Mech.E., M.Cons.E.
W. O. MANNING, F.R.Ae.S.
R. B. MATTHEWS, Wh.Ex., A.M.Inst.C.E., M.I.E.E., F.R.Ae.S.
Prof. A. L. MELLANBY, D.Sc., LL.D., M.I.Mech.E.
J. H. R. RATCLIFFE, B.Sc. (Eng., Hons.), M.I.Mech.E.
Col. C. W. D. ROWE.
W. A. SCOBLE, D.Sc., A.R.C.Sc., M.I.Mech.E.
P. W. SEEWER, D.E. (Zurich), M.Inst.C.E., M.I.Mech.E.
Prof. S. PARKER SMITH, D.Sc., M.I.E.E., A.M.Inst.C.E.
C. F. H. VERITY, A.M.Inst.C.E., A.M.I.E.E., A.M.I.Mech.E.
E. G. WALKER, F.C.G.I., B.Sc. (Eng.), M.Inst.C.E., M.I.Mech.E., M.Am.Soc.C.E.
Major F. L. WATSON, M.Inst.C.E., M.I.Mech.E.
G. WATSON, M.Inst.C.E., M.I.Mech.E.
C. H. WOODFIELD, M.I.Mech.E., M.I.Struct.E.
T. WRIGHT, Ph.D., M.Sc.
M. L. YATES, Ph.D., M.Sc.Tech., M.A. (Com.), M.I.Mech.E.

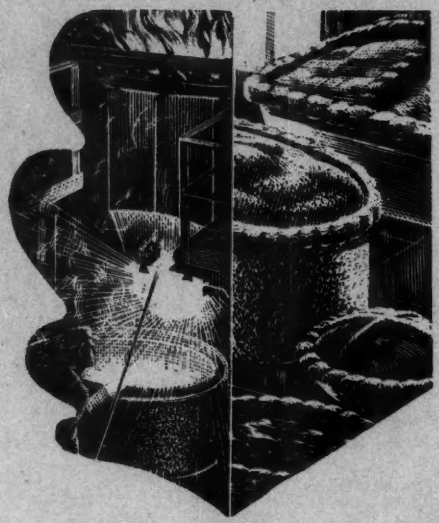

TOOL STEELS • ENGINEERS'
SMALL TOOLS • SAWS
MACHINE KNIVES

With Steel as with Pastry-*its all in the Making!*

Ask two cooks to make some pastry according to a certain recipe. The pastry they produce may look the same, but to the critical palate that of one cook will eat differently to that of the other.

And its the same with steel. For steel of a certain specification made by one firm will frequently behave quite differently in service from that made to the same specification by another firm. That is where the art of steel making comes in—an art never better practised than by the metallurgists and hereditary craftsmen of Sandersons' of Sheffield. For not only are Sandersons' Steels unsurpassed for their various purposes, but cast for cast, they maintain an amazing uniformity in quality.

Sandersons
of Sheffield

SANDERSON BROS. & NEWBOULD LTD.
ATTERCLIFFE WORKS SHEFFIELD

Telephone : Attercliffe 41201 (4 lines) *Telegrams : Sanderson, Sheffield*

CONTENTS

	page
Analysis of Small Motions by means of the Photo-Electric Cell *"The Engineers' Digest," Vol. 6, No. 6, page 156.*	156
An Apparatus for Investigating the Behaviour of Regulating Devices *"The Engineers' Digest," Vol. 6, No. 6, page 141.*	141
A Novel Automatic Synchronizer *"The Engineers' Digest," Vol. 6, No. 6, page 166.*	166
Brittleness and Ductility of Metals at High Temperatures *"The Engineers' Digest," Vol. 6, No. 6, page 148.*	148
Improvement of Engineering Carbon Steel *"The Engineers' Digest," Vol. 6, No. 6, page 155.*	155
Jet Propulsion Problems *"The Engineers' Digest," Vol. 6, No. 6, page 160.*	160
The Heating of Wire in Wire Drawing *"The Engineers' Digest," Vol. 6, No. 6, page 158.*	158
The Jalbert System of Air Blast Injection *"The Engineers' Digest," Vol. 6, No. 6, page 157.*	157
The New Limitherm Relay *"The Engineers' Digest," Vol. 6, No. 6, page 146.*	146
The Structure of Hard Metal Alloys *"The Engineers' Digest," Vol. 6, No. 6, page 164.*	164
Waste Heat Utilisation in Industry *"The Engineers' Digest," Vol. 6, No. 6, page 144.*	144
X-Ray High Tension Plant with Resonance Transformer *"The Engineers' Digest," Vol. 6, No. 6, page 154.*	154

ACTARC Heavy Duty ELECTRODE HOLDER

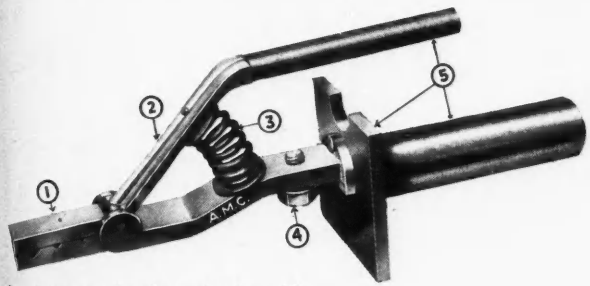

1. Jaws to take electrodes from 14g. to $\frac{3}{16}$ in. diameter.
2. Rigid lever arm.
3. Replaceable spring remote from source of heat.
4. Cable clamp as near the clamping jaws as possible to reduce resistance losses.
5. Handle insulators and guard of high-class fireproof material.

Manufactured from high conductivity bronze throughout.

Total weight 23 ozs.

Maximum current capacity 450 amps

This heavy duty Electrode Holder has perfect balance. The special material employed ensures long life and enables the holder to stand up to continuous heavy welding without overheating.

ACTARC SUREARC

ARC MANUFACTURING CO., LTD.

PROPRIETORS OF THE SURE ARC ELECTRODE CO., LTD

ACTARC WORKS, GOLDHAWK ROAD, LONDON, W.12

REGD. TRADE MARK

A.C.2

TELEPHONE: SHE 1151 TELEGRAMS: ACTIVARC, PHONE, LONDON. CABLES: ACTIVARC, LONDON

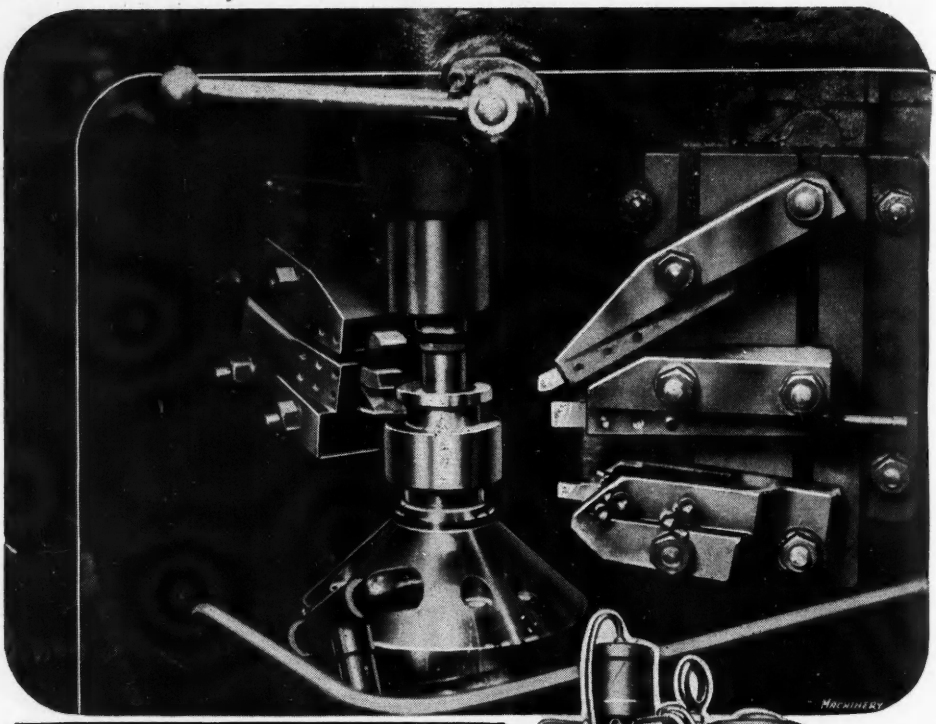

RYDERMATICS

for Maximum production

ON MULTI-TOOL JOBS

The illustration above shows a set up for the first turning operation on Tractor Transmission Pinions. The Rydermatic was originally developed for this type of work but large numbers have been supplied recently for work on various sizes of shell.

The machine can be supplied in two sizes, No. 18, with 60 h.p. motor, for heavy roughing operations; No. 12, with up to 25 h.p. motor, for lighter work. Unskilled labour can be employed, as the motions to be learned are few and tool setting is easily carried out, due to the extreme accessibility of all slides.

Maximum Swing 20 in. diameter.

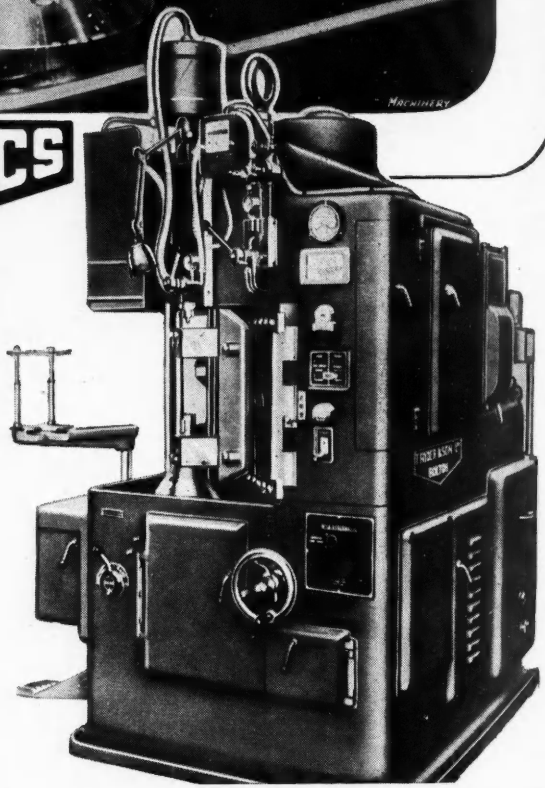

A.C. Wickman LIMITED

• COVENTRY • ENGLAND •

LONDON BRISTOL BIRMINGHAM MANCHESTER LEEDS GLASGOW NEWCASTLE

AN APPARATUS FOR INVESTIGATING THE BEHAVIOUR OF REGULATING DEVICES

By J. von FREUDENREICH. (From *The Brown Boveri Review*, July, 1944, p. 228-232).

As long as regulating devices remained relatively simple, their mathematical investigation was easily effected. The performances required of regulating devices, however, have increased steadily from year to year, the systems to be regulated becoming more and more complex and their mathematical investigation becoming correspondingly complicated. In principle, the mathematical treatment is simple. The equations of motion are set down for the different parts (machine, pipe-line, servo-motor gear, governor, etc.), and from these the equation of motion for the entire regulating arrangement is derived. The result is a differential equation of higher order, its order, as a rule, increasing with the number of component parts. But to be able to carry out a calculation at all, assumptions have to be made such that the coefficients of this equation can be treated as constants. This makes it possible to solve the equation and to answer all questions in regard to the performance of the governing system (stability, maximum deviation, time of regulation, etc.). As soon, however, as the order of the differential equation is higher than 3 or 4, the calculations become so extensive and involved that they generally have to be abandoned. There have, therefore, been many attempts to produce mechanical or electrical models, by the aid of which the problem can be readily solved experimentally. The mathematical investigation of a regulating arrangement consists fundamentally in the solution of a differential equation, hence any of the existing forms of integrating machines can be used for this purpose, and conversely an apparatus designed for investigating regulating systems is at the same time a device for integrating differential equations.

The machine described below was not designed with the intention of obtaining a high degree of accuracy, but rather with the object of retaining simplicity while enabling the factors which affect the stability of a governing system to be varied during operation. In this manner it is possible to find out very quickly which factors must be altered in order to improve the stability. In addition to this, it was required that the machine should also be capable of solving differential equations with variable coefficients.

THE EQUATIONS OF MOTION OF THE INDIVIDUAL COMPONENTS OF A GOVERNING SYSTEM.

(a) *Equation of a machine* (Fig. 1).—Let m denote the lift of the valve regulating the flow of the driving medium, m_{max} the maximum lift and μ the relative lift, i.e.,

$$\mu = \frac{m}{m_{max}}$$

Let us further denote by φ the value of the momentary deviation of the speed referred to the average speed ω_m.

$$\varphi = \frac{\Delta\,\omega}{\omega_m}$$

The equation of the machine is then

$$T_a\,\varphi' + H\varphi = \Psi\,\mu - \lambda \quad .. \quad .. \quad (1)$$

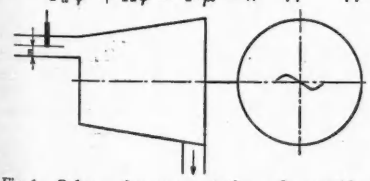

Fig. 1. **Schematic representations of a machine.**
m = Opening of the valve regulating the flow of the driving medium.

In this equation, T_a denotes the starting time of the machine, that is the time which would be required by the constant torque M_{max} to bring the unloaded machine from standstill up to normal speed, or

$$T_a = \frac{\Theta\,\omega_m}{M_{max}}$$

where Θ is the polar moment of inertia of the machine, and M_{max} the maximum driving torque. The quantity H is given by the " equalising effect " (self regulation), which indicates to what extent the energy supplied must be altered in order that the speed of the unregulated machine shall change by 1 per cent.

(b) *Equation of a pipe line* (Fig. 2).—Here also we

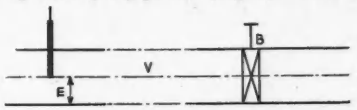

Fig. 2. **Schematic representation of a pipe line.**
m = Opening of the valve regulating the flow of the medium.
B = Valve regulating the outlet.
V = Volume of the pipe between regulating and consumer valves.

denote the lift of the valve by m, the volume of the pipe line between the regulating valve and the consumer's stop valve being V m³. The equation of the pipe line is then

$$T_1\,\pi' + H\pi = \Psi\,\mu - \lambda \quad .. \quad (2)$$

T_1 denotes here the filling time of the pipe line

$$T_1 = \frac{V\,\gamma_m}{G_{max}}$$

that is, the time during which the quantity G_{max} would have to flow in order to bring the pressure in the pipe line from zero to the normal value p_m with the consumer's stop valve closed. Further,

$$\pi = \frac{\Delta\,p}{p_m}$$

and H again the equalizing effect.

(c) *Equation of the governor.*—Modern governors which are not required to have a large work capacity, are built with small masses, and the friction at the pivots provides sufficient damping. Under these circumstances it can be assumed that the governor follows any changes of speed instantaneously. Let us denote the lift of the governor by y, and put

$$\eta = \frac{y}{y_{max}}$$

If the governor is in the uppermost position at the speed ω_{max}, and in the lowest position at the speed ω_{min}, then we may define the static drop as

$$\delta_r = \frac{\omega_{max} - \omega_{min}}{\omega_m}$$

and the equation of the governor is then

$$\eta = \frac{\varphi}{\delta_r} \quad .. \quad .. \quad .. \quad (3)$$

(d) *Equation of the servo-motor gear* (Fig. 3).—It is assumed that the speed of the piston is proportional to the lift s of the relay valve. If the relay valve is fully open (lift = s_{max}) the servo-motor piston travels the distance m_{max} in the time T_s. This is the closing time of the servo-gear motor. The lift of the relay valve depends not only on the lift of the governor y, but also on the lift of the recall point Z. The equation of the

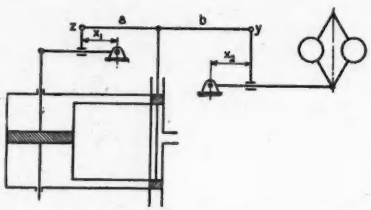

Fig. 3. Servo-motor gear with adjustable recall (x_1) and adjustable governor effect (x_2).

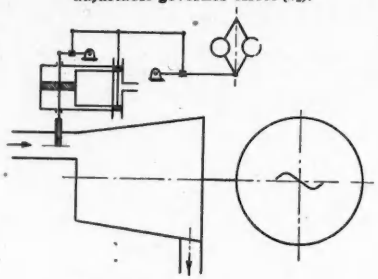

Fig. 4. Governing of a turbine with servo-motor gear.

servo-motor gear is then

$$T_s \mu' + R \mu = - A\eta \quad .. \quad (4)$$

The quantities R and A depend on the lever ratios x_1 and x_2.

THE EQUATION OF THE GOVERNING SYSTEM.

We shall consider first the simple case of the governing of a turbine with a servo-motor gear (Fig. 4). The equations of the individual components are given by equations (1), (3) and (4). If we eliminate from these η and μ there remains the equation of the governing system.

$$T_a T_s \varphi'' + (RT_a + HT_s)\varphi' + \left(\frac{A\Psi}{\delta_r} + HR\right)\varphi = - R\lambda \quad (5)$$

This is the equation of a damped oscillation.

If we compare the equations (4) and (1) we see that it is readily possible to replace the machine by a servo-motor gear. We connect up two servo-motor devices, as shown in Fig. 5, and obtain the following equations:

If by means of equation (4) we express η in terms of λ and μ_2, the equation of the first servo-motor system becomes

$$T_1 \mu_1' + R_1 \mu_1 = -B\eta_1 = -A_1\mu_1 - C_1\lambda$$

and that of the second:

$$T_2 \mu_2' + R_2 \mu_2 = + A_2 \mu_1$$

Substituting in the first equation the value of μ_1 given by the second we obtain

$$T_1 T_2 \mu_2'' + (R_2 T_1 + R_1 T_2)\mu_2' + (A_1 A_2 + R_1 R_2)\mu_2 = -C_1 A_2 \lambda \quad .. \quad .. \quad .. \quad (6)$$

This equation becomes identical to equation (5) when we put

$$\mu_2 = \varphi; \quad T_1 = T_a; \quad T_2 = T_s; \quad R_2 = R; \quad R_1 = H;$$

$$A_1 A_2 = \frac{A\Psi}{\delta_2}; \quad C_1 A_2 = R$$

The motion of the second servo-motor piston will therefore represent exactly the speed variation φ of the machine.

As a further example, the governing of a turbine of

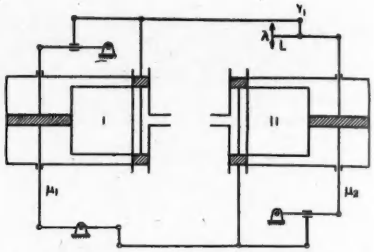

Fig. 5. Substitution of a servo-motor gear (II) for the machine.

The movement λ corresponds to the sudden application or removal of the load.

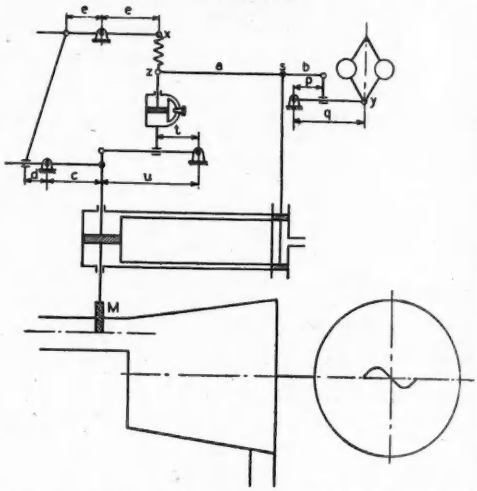

Fig. 6. Governing of a turbine with both permanent and temporary static drops adjustable.

The distance t varies the temporary and the distance d the permanent static drop.

which the permanent and the temporary static drop can be varied (Fig. 6) will be considered.

Making $d/c = R_b$, $t/u = R_v$, and if k_t denotes the spring constant (spring force/lift), k_l the constant of the oil dashpot (force acting on the piston/speed of piston relative to casing), $T_1 = k_l/k_t$, then the equation of the servo-motor gear is

$$T_s T_1 \mu'' + (T_s + R_v T_1)\mu' + R_b \mu = - (T_1 \eta' + \eta) \; .. \; (7)$$

where the lever ratios are so chosen that

$$\frac{m_{max}}{s_{max}} = \frac{a+b}{b}; \quad \frac{m_{max}}{y_{max}} = \frac{a}{b} \cdot \frac{p}{q}$$

The equation of the governing system is then

$$T_a T_s T_1 \varphi''' + [T_a(T_s + R_v T_1) + HT_s T_1]\varphi'' + [R_b T_a + \frac{\Psi}{\delta_r} T_1 + H(T_s + R_v T_1)]\varphi' + \left[\frac{\Psi}{\delta_2} + HR_2\right]\varphi = -R_b\lambda \quad (8)$$

It is seen that the mathematical calculation of this case involves a large amount of work. The corresponding equivalent combination of servo-motors is represented in Fig. 7.

If the lever ratios are suitably chosen, the above two servo-motor gears reproduce the equation (7) and the combination of the three servo-motor gears the governing equation (8). In this manner it is possible to represent every governing problem by means

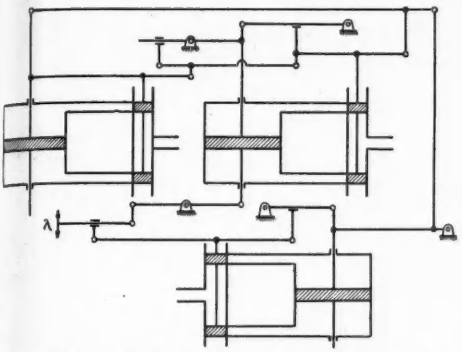

Fig. 7. **Governing of a turbine corresponding to Fig. 6.** Turbine and oil-dashpot are replaced by servo-motor gears.

of servo-motor systems. In the above examples, a hydraulic servo-motor has been chosen for the sake of facility of representation. The apparatus described below, on the other hand, is purely mechanical.

MECHANICAL SERVO-MOTOR GEAR.

In the mechanical servo-motor gear illustrated in Fig. 8 the drum T rotates at constant speed. The lever B, which is pivoted at the point 0, carries on a pivot mounting the small roller C. The axis of this roller can be rotated by the link mechanism $DEFG$, so that the roller makes an angle with the length axis of the drum. The velocity with which the lever B is carried forward is proportional to the tangent of the angle which the axis of the roller makes with the axis of the drum. The tilting of the roller is effected by means of the slide H, which carries the slotted lever along with it. The tangent of the angle of the lever K, and therefore of the roller, is proportional to the travel of the slide. Denoting the

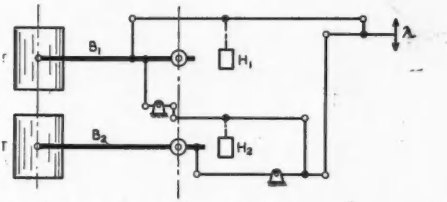

Fig. 9. **Combination of two mechanical servo-motor gears to represent a differential equation of the second order with constant coefficients.**
H_1 and H_2 are the control slides, λ the disturbance function.

travel of the slide by s and the travel of the end of the lever B by x, then we obtain the equation

$$x' = -Cs \quad .. \quad .. \quad .. \quad (9)$$

We can insert here also the relative values

$$\xi = \frac{x}{x_{max}}; \quad \delta = \frac{s}{s_{max}}$$

and can write the equation (9) in the form

$$T_s \xi' = -\sigma \quad .. \quad .. \quad .. \quad (10)$$

This is exactly the equation of a servo-motor gear without recall device. The direction of rotation of the drum may be chosen such that as in the case of a servo-motor, the direction of travel of x is opposed to that of s. If we add a recall arrangement, we obtain again equation (4).

Fig. 9 represents once again the simple control system corresponding to Fig. 4, but this time with mechanical servo-gear. The drums are denoted by T, the levers which carry the rollers are B_1 and B_2; and H_1 and H_2 represent the control slides causing the tilting of the roller axis. The levers transmitting the movements must be light in weight. Further, all pivot points must either be of the needle point or of the ball bearing type in order that the resistance shall be as small as possible.

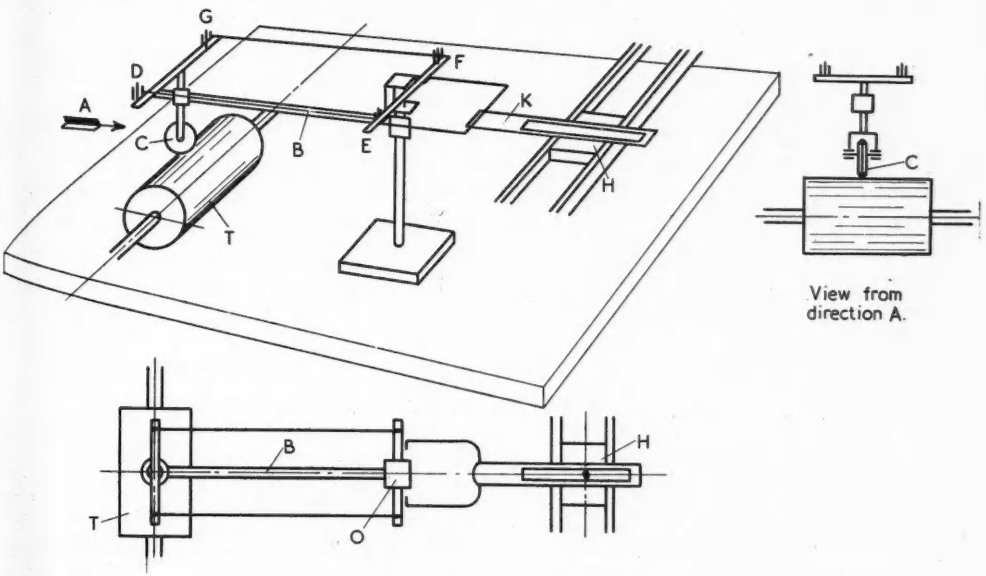

Fig. 8. **Mechanical servo-motor gear.**
The axis of the roller C, which runs on the drum T rotating at constant speed, can be tilted by means of the slide H whose motion is transmitted by the link mechnaism D G F E. This causes the lever B to move about the pivot O.

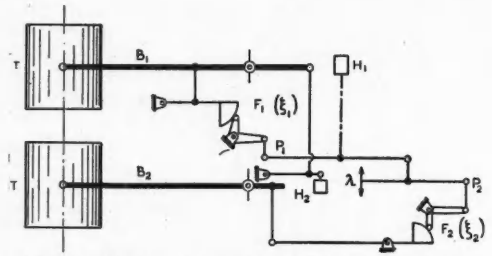

Fig. 10. Combination of two mechanical servo-motor gears to represent a differential equation of the second order with variable coefficients.

The coefficients are functions of the motions of the levers B_1 and B_2. The motion of λ corresponds to the disturbance function.

APPLICATION OF THE APPARATUS TO THE INTEGRATION OF DIFFERENTIAL EQUATIONS.

It has been seen that when two sets of apparatus are combined as in Fig. 5 they reproduce a differential equation of the second order (equation 6). This equation (6) has constant coefficients, and it corresponds to the damped oscillation of a mass

$$M\frac{d^2x}{dt^2}+c\frac{dx}{dt}+kx=D\lambda \quad .. \quad .. \quad (11)$$

where λ may be any particular function of the time. In this particular case, the damping has been assumed to be proportional to the velocity and the spring action proportional to the displacement. If two cams are introduced of such shape that the lift of the point P_1 is any given function of ξ_1, i.e., $F_1(\xi_1)$ and the lift of the point P_2 any given function of ξ_2, i.e., $F_2(\xi_2)$, then the equation of the first servo-gear is

$$T_1\xi_1'=-AF_1(\xi_1)-BF_2(\xi_2)+D\lambda$$

and that of the second

$$T_2\xi_2'=C\xi_1$$

On substituting the value of ξ_1 given by the second equation in the first one, we obtain the equation of the system, namely

$$T_1T_2\xi_2''+aF_1(\xi_2')+bF_2(\xi_2)=D\lambda \quad .. \quad .. \quad (12)$$

In this manner it is possible to build up apparatus to reproduce any differential equation. It should, however, be noted that the functions which are introduced can only be functions of ξ or of its derivatives and not of any other variable.

If it is required that the coefficients shall also be functions of the time, it is necessary to proceed as follows (Fig. 11) :—

Only the drums of the parts II and III are driven at constant speed, while the drum I is driven from the lever II by means of a string passing over rollers. The angle through which the drum turns is then proportional to the travel of the lever II. Similarly the drum IV is

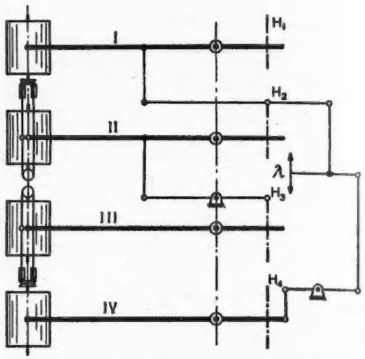

Fig. 11. Combination of four servo-motor gears for representing a differential equation of the second order with variable coefficients which may be functions of both the time and of the movement of the levers.

H_1—H_4 are the control slides, λ the disturbance function.

driven by the lever III. The equation for the second apparatus is

$$T_2\xi_2'=-\sigma_2=-A\xi_1-B\xi_4+D\lambda$$

and that for the third

$$T_3\xi_3'=C\xi_2$$

Differentiating the first equation we obtain

$$T_2\xi_2''=-A\xi_1'-B\xi_4'+D\lambda'$$

The velocity ξ_1' is proportional to the speed of the drum I, that is, proportional to ξ_2', and proportional to the travel of the control slide σ_1 :

$$\xi_1'=c_1\xi_2'\sigma_1$$

and similarly

$$\xi_4'=c_2\xi_3'\sigma_4$$

hence

$$T_2\xi_2''=-a\xi_2'\sigma_1-b\xi_3'\sigma_4+D\lambda'$$

If we insert the value of ξ_2 given by the equation of the third apparatus, we obtain

$$T_2T_3\xi_3'''+a\sigma_1T_3\xi_3''+Cb\sigma_4\xi_3'=CD\lambda'$$

or

$$T_2T_3\xi_2''+aT_3\sigma_1\xi_2'+Cb\sigma_4\xi_2=T_3D\lambda'$$

It is then possible to move the control slides s_1 and s_2 in any manner, according to a function of ξ or of the time or of both together. We have, therefore, quite generally

$$T_2T_3\xi_2''+\Phi_1.\xi_2'+\Phi_2.\xi_2=F(t) \quad .. \quad (13)$$

where Φ_1 and Φ_2 may be any functions of the time and of their derivatives. If additional elements are available, differential equations of higher order can also be integrated.

The apparatus here described is not a precision instrument which gives solutions with a high degree of accuracy ; it does, however, enable a general picture of the solution to be quickly obtained by simple means.

WASTE HEAT UTILISATION IN INDUSTRY

By A. AHLSTRÖM. (From *Tekmisk Tidskrift*, Vol. 75, March 17, 1945, p. 307-314.)

THE fact that some 70 per cent of Sweden's fuel consumption must be imported from abroad, makes it necessary to utilise waste heat to the greatest possible extent. As about 30 per cent of the country's industrial fuel consumption is accounted for by the iron ore, paper and cellulose industries, waste heat utilisation in these industries will be dealt with first.

Prof. L. Malm has recently made a thorough investigation into the possibilities of extracting waste heat from the products of combustion in the iron and steel industries.* He has shown that the heat which annually goes to waste with the products of combustion of iron and steel plants corresponds to the calorific value of 278,000 tons of bituminous coal. Prof. Malm estimates that an equivalent of some 200,000 tons of coal is recoverable from the waste gases of these industries. To-day only a fraction of this amount is being recovered, partly in waste heat boilers and partly in air preheaters.

In the waste heat boilers installations the steam

* *Jernkontorets Annaler*, 1943, p. 389.

generated is used for space heating purposes, while the hot air delivered from the air preheater is used as combustion air for furnaces. In certain cases, hot air is also used for space heating purposes. The quantities of heat required for space heating are, however, far too seasonal to permit an efficient utilisation of waste heat extraction plants. More satisfactory is the position, as far as combustion air requirements are concerned, as these are not subjected to seasonal variations. Prof. Malm suggests that in plants where the available waste heat is in excess of combustion air and space heating requirements, the available excess heat should be utilised for the generation of electric energy. Assuming 1 ton of steam to be the equivalent of 600,000 kcal, the capital cost of a waste heat boiler of the forced circulation type is estimated by Prof. Malm at about 100,000 kroner per ton of steam produced per hour, the corresponding figures for ordinary boilers and air preheaters being 70,000 and 55,000 kroner respectively. These costs were estimated on the basis of installations with a steam output of 2 to 6 tons per hour. In waste heat boiler and air preheater installations, it is not an economical proposition to cool the gases to such an extent that their dewpoint is reached. On the contrary, care must be taken to preclude any possibility of the gas temperature decreasing to a point at which condensation and consequent corrosion can occur.

Cooling of the waste gas below its dewpoint may, however, be of advantage in certain cases, especially where fuels of high moisture content are burned. But this mode of operation calls for an entirely different type of heat extracting apparatus of the direct contact type as outlined in Fig. 1. In this device, which combines gas washing with waste heat extraction, the gases are passed over a number of perforated plates which are wetted by a descending stream of water. The heated water is passed through a heat exhanger to yield a portion of its sensible heat, and is subsequently returned to the plate tower for reheating.

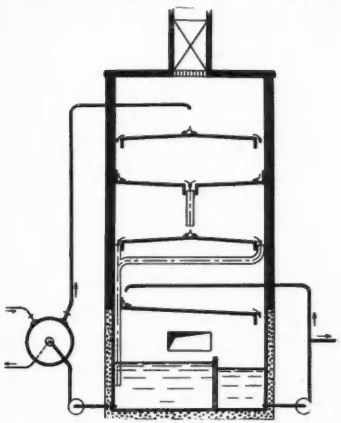

Fig. 1. **Combined gas washer and direct contact type heat exchanger.**

A waste heat extraction plant of this type installed in a Swedish sulphate works has a capacity of 26,600 cu. m. N.P.T. of waste gas per hour, with a water circulation of 5,450 kg. per hour. By reducing the gas temperature from about 67 deg. C. to 45 deg. C., some 6 tons are produced per hour, hereby recovering about 65 per cent of the waste heat contained in the gases. The capital cost of this plant was about 120,000 kroner, that is, 20,000 kroner per ton of steam produced per hour.

Fig. 2 shows the diagrammatic layout of a plant for the utilisation of the exhaust steam available from the steam hammers of a steel mill. Here the exhaust from the hammers will first be passed through a scrubber in which a certain amount of condensation will occur. The steam discharged from the scrubber will then be admitted to a jet condenser to obtain complete condensation. The water heated in the condenser will be passed into the scrubber for final heating and for degasification, and will then be delivered to the upper part of an accumulator. The average steam load will amount to 5 tons per hour. The cost of the complete plant is estimated as 20,000 kroner, equivalent to 4,000 kroner per ton of steam per hour capacity.

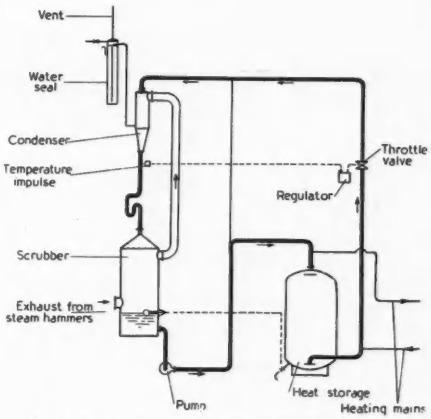

Fig. 2. **Utilisation of steam hammer exhaust.**

In the paper and cellulose industries very large amounts of heat are required for drying processes, and efficient waste heat utilisation is therefore of the greatest importance. The waste heat discharged from the drying machinery is contained in air which is more or less saturated with moisture. Any reduction in air consumption therefore leads to a rise in the saturation temperature and increases the possibilities of waste heat recovery. The achievement of highest efficiency in the dryer section of a paper machine must therefore be considered a foremost task. According to G. Edling, a better utilisation of the waste heat available in paper machine operation will be achieved by adopting the layout shown in Fig. 3. This scheme envisages the employment of air heaters of the extended surface type and of water heaters of the scrubber type.

A vacuum type evaporator originally designed for the evaporation of whey in dairy plants is outlined in Fig. 4. This type of evaporator is now also in use for the evaporation of blood, milk, glue, and a few other

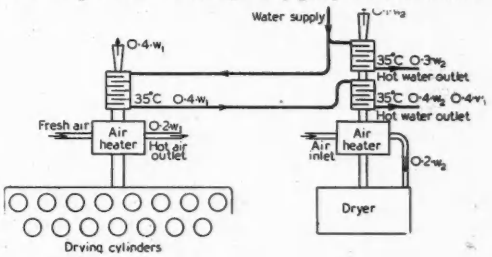

Fig. 3. **Waste heat utilisation in paper machine installation equipped with drying cylinders and air dryer.**

W_1 = heat supplied to cylinders,
W_2 = " " " air dryer.

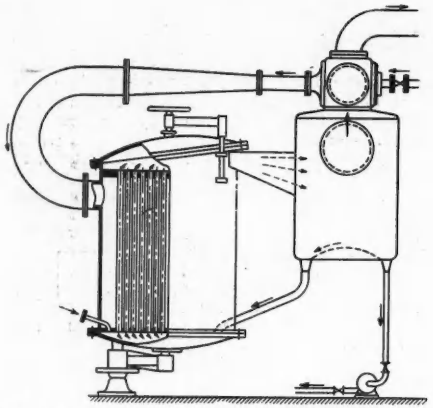

Fig. 4. **Vacuum-type evaporator equipped with steam jet compressor.**

products. In this apparatus a portion of the secondary steam is re-compressed by means of a steam jet compressor operated by live steam. In an actual test 0.52 kg. of steam were required per kg. of water evaporated. In this test the whey was admitted with a temperature of 30.2 deg. C., and the temperature in the evaporator was 71.2 deg. C. The primary steam pressure at the inlet of the steam jet compressor was 6.36 atm.g.

Waste heat in the form of sensible heat in liquids exists in the condensate of steam consuming apparatus and machinery. If this waste heat is to be utilised by means of a heat exchanger, the condensate discharge should be arranged as shown in Fig. 5, in order to maintain a constant water level.

The heating system fitted to the drying cylinders of a modern paper machine, which is diagrammatically shown in Fig. 6, furnishes another striking example of the thermal economies that can be effected. Referring to the diagram, the dryer section is seen to be subdivided into two cylinder groups passed by the steam in series-flow. The larger of these two groups is heated by high pressure steam, while the smaller group is vacuum-heated by using the exhaust from the high-pressure group.

In steel works practice, considerable amounts of waste heat may be extracted from the cooling water discharge from blast furnaces, high frequency furnaces, etc. Thus, for instance, the cooling water discharged from the cooling circuit of an open-hearth furnace carries off some 1,200,000 kcal. per hour. In steel furnace practice, the temperature of the discharged cooling water generally ranges from 90–95 deg. C. This cooling water can therefore be used to advantage for space heating purpose.

The layout of a waste heat recovery system operated in conjuction with a forging furnace is given in Fig. 7. Cooling water is circulated through the door frames and the flue gas damper of the furnace, and then used for space heating purposes. Tests have shown that the recovered heat may amount to as much as 20 per cent of the calorific value of the fuel.

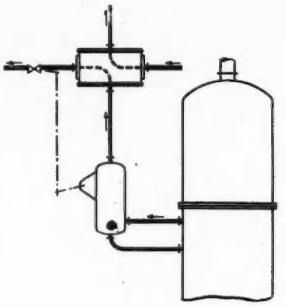

Fig. 5. **Condensate cooler with correctly placed drain connection.**

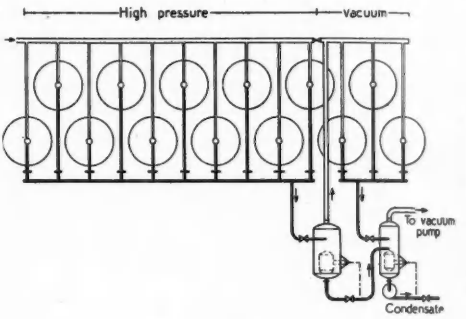

Fig. 6. **Condensate removal system for pulp dryer (cylinder type).**

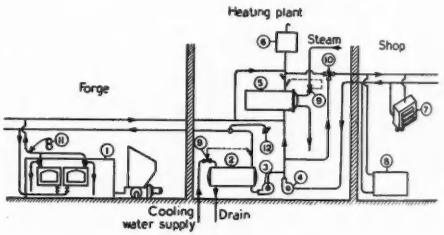

Fig. 7. **Space heating with utilisation of cooling water from forging furnace.**

(1) Furnace with water-cooled door frames.
(2) Heat exchanger.
(3) Circulating pump.
(4) Pump operating the heating circuit.
(5) Heat exchanger.
(6) Expansion vessel.
(7) Fin-type space heater.
(8) Radiator.
(9) Thermostat-controlled valve.
(10) Mixing valve.
(11) Thermometer with alarm device.
(12) Flow meter.

THE NEW LIMITHERM RELAY.

By O. NAEF and T. IMHOF. (From *Bulletin Oerlikon*, No. 247, January/February, 1944.)

THERMALLY actuated overload protective equipment, the application of which was formerly limited to small electric motors, is now being also applied on an increasing scale to larger machines and apparatus in order to utilise their capacity to the highest permissible degree. It goes without saying that the limiting factor in this respect is the maximum temperature which the electric conductors can be permitted to attain if damage to the insulation is to be avoided. It is also well known that the rise in the temperature of the conductors exhibits a time lag with respect to the changes in heating effect, that is, the load variations. Neither definite-time nor inverse-time overload relays take into account the mitigating influence of this thermal inertia, and they cannot therefore be considered as suitable protection in cases where large load variations are encountered.

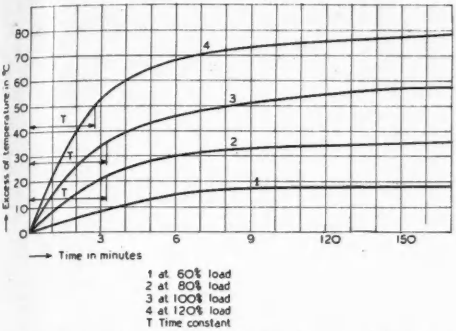

Fig. 1. Measured temperature rise characteristics of a machine showing the variation of the time constant with the load.

To be effective the protective equipment should register the temperature rise to its permissible maximum level in a reliable manner ; but it should maintain uninterrupted operation under overload conditions as long as the limiting temperature level is not actually exceeded. These requirements are met by the Limitherm relay because it represents a thermal replica of the apparatus or machine which it protects. The employment of this type of relay is therefore especially indicated where the loading carried by the equipment to be protected is subject to frequent large fluctuations. Typical cases of this kind occur in the operation of self-starting synchronous motors and of comparatively large squirrel cage motors. Load conditions of this kind are also encountered in rolling mill drives, particularly in those of the reversing type in which the temperature rise of the driving motor is largely governed by the frequency of the peak load. Similar conditions may be found in the case of cables carrying highly variable loads or in the case of transformer supplying distributing systems with periodically occurring peak loads. Still another example is the operation of electric furnaces.

The salient features of the Limitherm relay may be summarised as follows :—

(1) Close adaptation to the termperature rise characteristic of the equipment to be protected.

(2) A power consumption small enough to permit connection of the relay to normal current transformers in conjunction with other instruments.

(3) Constant supervision of the equipment to be protected by—

(*a*) Visual indication of the momentarily prevailing thermal loading in percentage of the nominal current.

(*b*) Snap-action if a selected percentage value of the maximum thermal loading is exceeded.

(4) Compensation for ambient temperature conditions.

(5) Possibility of increasing the load limit in cases where a low temperature cooling medium is employed.

(6) Short-circuit protection by an adjustable instantaneous device.

(7) Facility of testing the relay.

Referring to point (1), it is known that the time-temperature characteristic of a homogeneous body subjected to a constant supply of heat can be represented by the function $\vartheta = \vartheta_{max}\left(1-e^{-\frac{t}{T}}\right)$ where ϑ is the temperature rise at the point of time t, ϑ_{max} is the final temperature rise and T is the so-called time constant. This time constant is defined as the time after

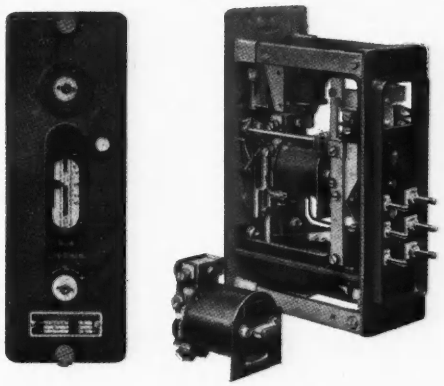

Fig. 2a. Fig. 2b.

Limitherm Relay.

(*a*) front view and (*b*) without housing. (A separate heater body in foreground.)

which 63.4 per cent of the final temperature rise are reached. However, all electrical machinery and apparatus, cables, etc., are heterogeneous bodies in thermal respects, each one of the different component materials having its influence upon the shape of the time-temperature characteristic. The conductor itself, the temperature of which is naturally of preponderant influence, therefore possesses a time-temperature characteristic which more or less deviates from the aforementioned theoretical time-temperature function. Especially at the beginning of the heating period does the time-temperature characteristic of the conductor exhibit a steeper rise, the conductor temperature rising more rapidly than that of the surrounding medium. This divergence increases with rising overload and is reflected by a diminution of the time constant as illustrated by Fig. 1. The nominal time constant is therefore defined as the time after which at rated load a temperature rise to 63.4 per cent of the limiting temperature rise is attained.

In the Limitherm relay shown in Fig. 2, indication as well as constant actuation are effected by the deformation of a metal bundle heated by a current which is proportional with the load current. The mass of metal required to produce a sufficiently large time constant is provided in the shape of a hollow cylinder enveloping the bimetal element and heating the latter in the main by radiation. Provision is also made for additional *direct* heating of the bimetal element. This increases the steepness of the temperature rise characteristic in the case of larger overload, thus taking account of the variations in the time constant as they occur in the equipment to be protected. Limitherm relays are built for time constants of 15, 30, 45 and 60 minutes. Typical time constants of electric motors of various capacities are given in the subjoined table.

TIME CONSTANTS OF ELECTRIC MOTORS.

H.P.	Speed r.p.m.	Time constant T minutes
Up to 100	—	10 — 25
100 to 300	3,000	15 — 30
do.	1500—750	20—40—60
do.	750—350	25—40—90
300 to 1000	3,000	20—30—45
	1500—750	30—40—60
	750—375	60—90—120

BRITTLENESS AND DUCTILITY OF METALS AT HIGH TEMPERATURES.

By W. SIEGFRIED. (From *Technische Rundschau Sulzer*, 1945, No. 1; p. 43–79.)

UNTIL quite recently the determination of the high temperature strength of steels was generally based upon the methods employed in short time testing at room temperature. The creep strength was arbitrarily established as the stress which after a certain duration of stressing, as e.g. after 25 hours, produced a creep rate not exceeding a specified maximum value. It goes without saying that the method of testing was far too simple to render a true acount of the physical phenomena involved; and it is not therefore surprising that component parts dimensioned on the basis of such short time test were found on more than one occasion to fail on actual service, and this without exhibiting any significant deformation prior to failure. Detailed examinations have proven that such failures were directly due to the choice of an unduly high working stress determined by short time test. Determination of the permissible working stress on the basis of long time tests of several thousand hours' duration is therefore essential.

The explanation of the seemingly inexplicable phenomena involved has been considerably advanced by observing the differences in the behaviour of smooth test bars on the one hand and notched test bars on the other. It was found that the notched test pieces made of certain steels exhibit a greatly inferior strength under low stress or under long time load as compared to the strength recorded with the notch-free piece. This behaviour can be taken as a clear indication of brittleness. Steels are known to exist, as for instance, the artificially aged Thomas steels, which exhibit this characteristic even at room temperature, whjle a ductile material will show exactly the opposite characteristic.

It can therefore be concluded that the behaviour of a steel under stress at elevated temperature is characterised by two strength values, namely its resistance to deformation and its resistance to fracture. Of these the resistance to deformation can be defined as the limiting stress under which a cessation of creep eventually takes place, while the resistance to fracture is represented by the load resulting in deformation-less fracture after an infinite length of time. Resistance to deformation can be ascertained by a short-time test, but resistance to fracture must be determined by a long time test lasting several thousand hours until fracture actually occurs. The theory of the intercrystalline criterion cohesion as originated by Rosenhain and Ewen is well adapted to furnishing the explanation of these phenomena; and on this basis the rapid decrease in the strength of a notched piece may be taken to be due to the same cause responsible for the deformation-less failure of notch-free test bars of steel under long time stress.

In this connection attention must be drawn to the fact that large tensile stresses which cause failure within a short time are known to produce a considerable reduction in area at the point of fracture, while long-time fracture under small stress is accompanied by a small reduction in area. Moreover, the reduction in area produced by long time loading will be the smaller the stress, that is, the longer the time to fracture. In first approximation it may be said that when highly stressed, the material fails because of insufficient resistance to deformation, while the fracture of the low stressed material is caused by a deficiency in cohesive strength. The task therefore was to obtain additional proof of the validity of this concept and to determine whether and how this concept could be made to form the basis of a new method of testing.

Another matter to be investigated in this connection was the nature of the embrittlement fracture and especially the question whether transcrystalline fracture is actually due to a combination of structural and mechanical phenomena. Still another point to be clarified was the significance of the elongation and contraction of the material in the high temperature long time test. Finally the physical phenomena occurring in notched bars subjected to static tensile load at elevated temperature had also to be investigated.

In view of the magnitude of the task and of the complexity of the test apparatus required to carry out high temperature creep tests, a way of procedure had to be evolved which would secure a maximum of results without requiring an excessive amount of equipment or an undue length of time. In view of the fact that certain alloys of tin and cadmium exhibit intercrystalline fracture under long time load at room temperature, it was decided to employ alloys of this type as far as fundamental investigations were concerned. This permitted a considerable simplification of the testing equipment. Before this step was taken, however, a number of tests had to be made so as to ascertain whether the behaviour of the tin and cadmium alloys at room temperature is comparable to that of steels operating at elevated temperature.

EXPERIMENTS WITH TIN-CADMIUM ALLOYS.

A first series of tests was conducted on an alloy composed of 94 per cent tin and 6 per cent cadmium. From the Sn-Cd equilibrium diagram established by Hansen and Pell-Walpole it is known that above 130 deg. C. this alloy consists mainly of an intermediate β phase. If the alloy is held at 168 deg. C. for some considerable time, it will therefore consist of a β phase which during cooling will undergo eutectoid decomposition at 130 deg. C. By heating the alloy to 120 deg. C. for some considerable time, an almost pearlitic arrangement of the α and γ phases can be obtained. Fig. 1 shows the microphotograph of a transversal section of a piece which was heated for 24 hours at 168 deg. C. subsequently quenched and then heated at 120 deg. C. for 24 hours; while Fig. 2 shows a specimen obtained in the identical way, but cold-worked at a temperature below 120 deg. C. Referring to Fig. 1, pearlite-like distribution of the α and γ phases is seen to obtain, but in the case of the cold worked material, Fig. 2, the γ phase is seen to be contained in globular formations embedded in the α matrix.

The results of the long-time rupture tests conducted on specimens of this material are charted in Figs. 3 and 4, the test bar dimensions being given in Fig. 5. Rate of strain vs. stress characteristic of the material is charted in Fig. 6 on the log-log scale,* and it will be noted that both curves exhibit a pronounced point of inflection. In the case of the heat treated alloy this point is seen to occur with a stress of approximately 240 kg. per sq. cm., while in the case of the cold worked specimen the inflection takes place under a load of some 120 kg. per sq. cm.

With loads ranging below the inflection point the strain rate was observed to tend toward stabilisation at a constant value, but with loads in excess of the inflection point, a progressive increase in the strain rate was noted.

The results obtained permit the drawing of the following conclusions: In both the cold worked and the heat treated state the strain characteristic of the notched piece intersects that of the notch-free piece. This must be taken to indicate the existence of a physical law much more far-reaching than was hitherto assumed. Hitherto this phenomenon had been observed only in the case of low alloyed steels stressed at temperatures of about 500 deg. C. The fact that tin alloys under

* See page 151.

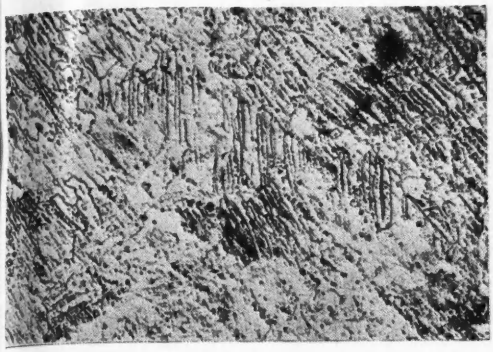

Fig. 1. **Microphotograph of transversal section of tin-cadmium alloy in heat treated condition.** Magnification 120 ×

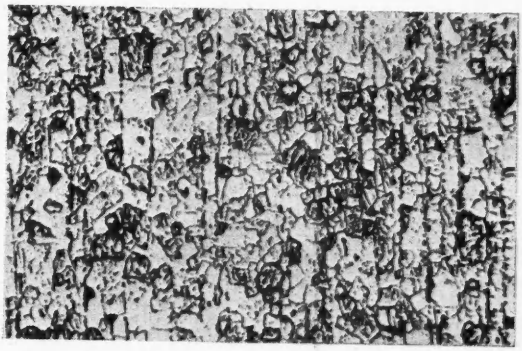

Fig. 2. **Microphotograph of transversal section of cold drawn tin-cadmium alloy.** Magnification 120 ×

Fig. 3. **Results of time-to-rupture tests on cold-drawn test bars.**

- Time-to-rupture characteristic of the notched bars.
- Time-to-rupture characteristic of the notch-free bars.
- ψ Reduction in area, per cent.
- δ_{gl} Deformation-free elongation, per cent.
- δ_e Elongation with deformation, per cent.
- $\delta 5$ Elongation at fracture, per cent.

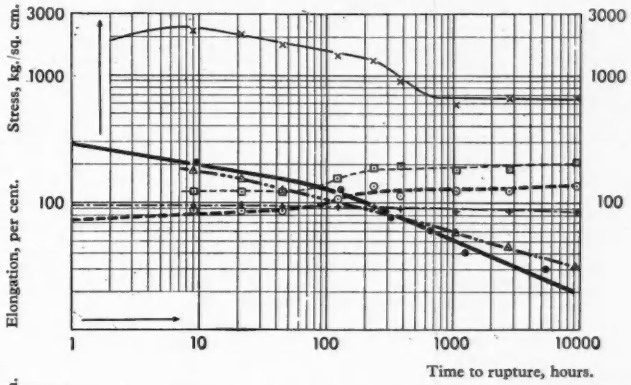

Fig. 4. **Results of time-to-rupture tests on heat treated test bars.**

- Time-to-rupture characteristic of the notched bars.
- Time-to-rupture characteristic of the notch-free bars.
- ψ Reduction in area, per cent.
- δ_{gl} Deformation-free elongation, per cent.
- δ_e Elongation with deformation, per cent.
- $\delta 5$ Elongation at fracture, per cent.

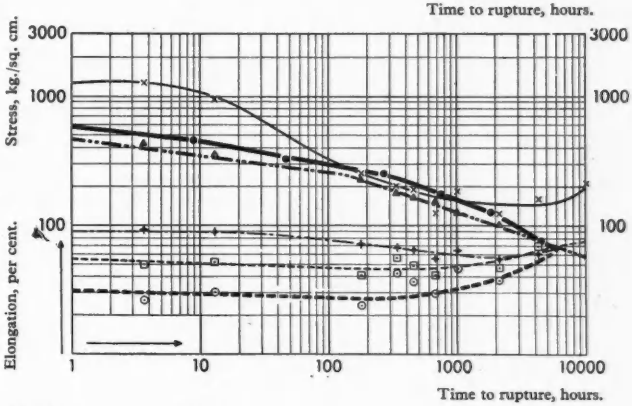

room temperature conditions behave in identical manner must therefore be taken as an indication that these phenomena represent a fundamental characteristic of the creep of metals.

For the purpose of clarifying the phenomena that result from the stressing of notched test bars, another heat of 94 per cent tin and 6 per cent cadmium was prepared and the entire heat was heat treated in the way described above. In order to study the influence of the depth and the radius of the notch, twelve different types of notches were used. An exploration of the influence of the angle of the V-notch was likewise considered important. By varying the type and dimensions of the notch both the tri-axial stress distribution in the interior of the test bar and the stress

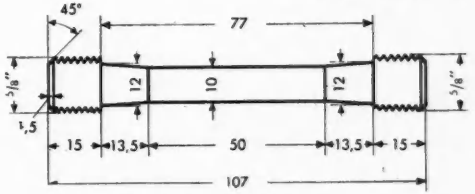

Fig. 5. **Test bar dimensions.**

concentration at the bottom of the notch may be varied. It was therefore hoped that the results obtained with various types of notches would furnish an indication

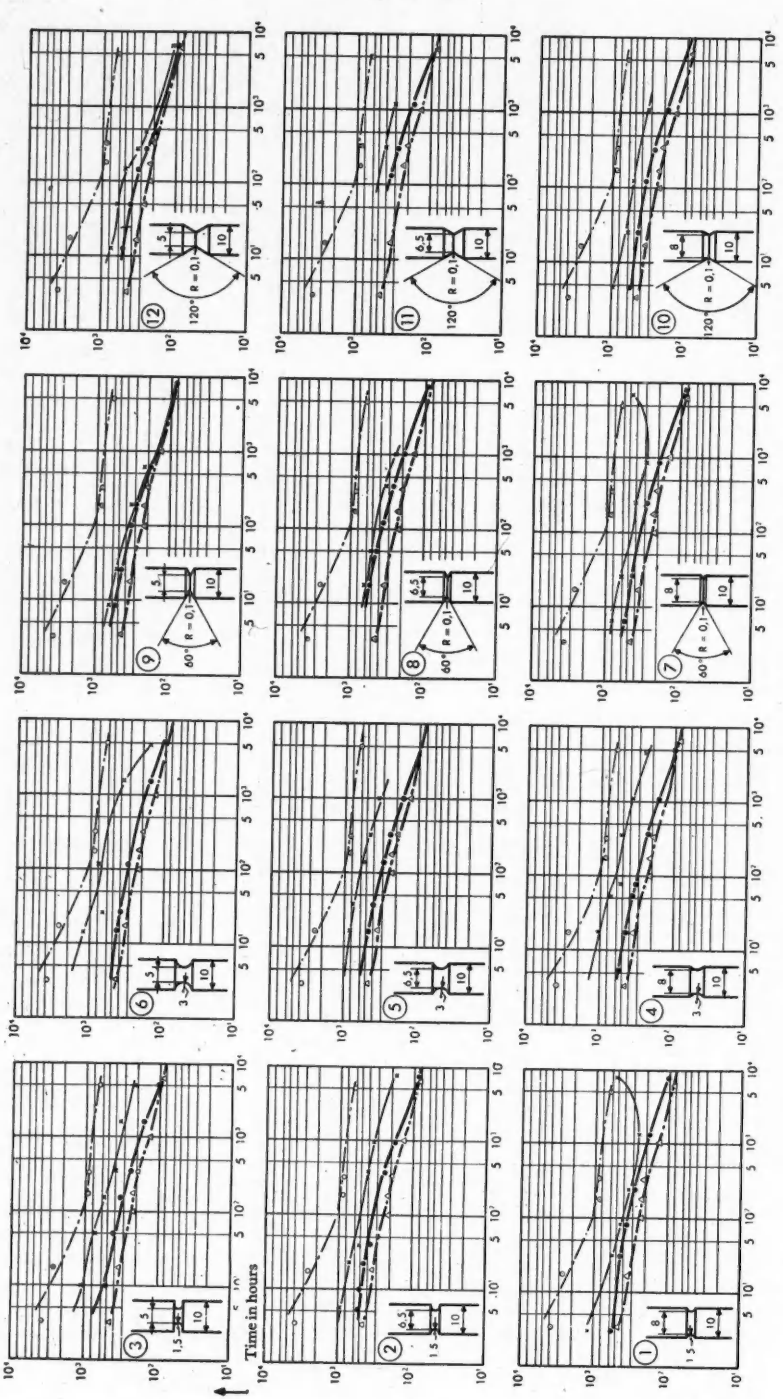
Stress kg./sq. cm.
Time in hours
Nominal stress in notched bars
Nominal stress in notch-free bars
True stress at fracture of notch-free bars
True stress at fracture of notched bars

Fig. 7. **Nominal stress and effective stress at moment of fracture as function of time to rupture.**

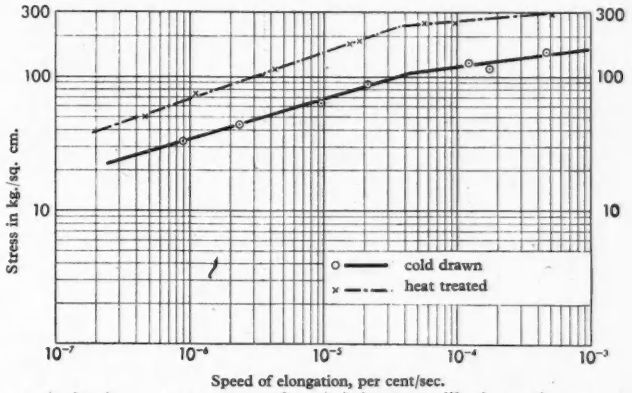

Fig. 6. **Stress versus creep characteristics (on log-log scale).**

as to whether the tri-axial stress distribution or the local stress concentration are the cause of embrittlement failure.

The time-to-rupture characteristics obtained for a number of different notches are charted in Fig. 7, each graph also containing the corresponding characteristic of the notch-free bar. The true stresses prevailing at the moment of fracture are also charted for both the notched and the notch-free specimens. These curves provide a measure of the cohesive strength of the bar at the moment of failure. From a comparative study of the various characteristics charted, it will be seen that quite irrespective of the shape of the notch the time-to-rupture curve of the notch-free specimen approaches that of the notched bar as the time-to-rupture is increased. It is seen that if the latter time is sufficiently extended, actual intersection of the two curves takes place. It will further be noted that the approach of the two curves does not proceed in a gradual manner, but that the time-to-rupture curve of the notched bar diverges a little from that of the notch-free bar before intersection takes place. The relative incidence of the two curves is therefore quite small at the point of actual intersection, so that it is difficult to determine accurately the point of time at which intersectiin takes place. This peculiarity is explained by the large deformation which, during the course of the test, completely alters the original shape of the notch.

The various charts given in Fig. 7 also show that with a greater depth of notch the points of intersection of the notch-free with the notched bar characteristics advance towards earlier times-to-rupture points.

A comparison of the characteristics of notches of different shape but of equal depth as given in the charts 3, 6 and 9 of Fig. 7, reveals that the Vee notch referred to in chart 9 causes a more rapid downward slope of the time-to-rupture characteristic than that produced by the notches of blunter shape referred to in the charts 3 and 6. It may therefore be concluded that the downward slope of the time-to-rupture curves which sets in after long time stressing of notched bars is chiefly due to the action of the prevailing triaxial stresses in the interior of the material. By charting the reduction in area at the moment of fracture versus the time-to-fracture, it is found that an increase in the depth of the notch; that is to say, an increase in the triaxial stresses, leads to a decrease in the reduction of area at the time of fracture, if the time-to-rupture is increased by reducing the loading of the bar. This is explained by the fact that the occurrence of intercrystalline failure is accelerated by an increase in the triaxial stress.

The data obtained from the investigations of the tin-cadmium alloys make it possible to form a conception of the phenomena attending the creep of a metal under stress ; and it must be concluded that the occurrence of embrittlement will always have to be reckoned with in cases involving creep at high temperature. If it is considered that the tin-cadmium alloys exhibit excellent ductile properties in the ordinary short time tensile test having reductions in area as large as 90 per cent, it is indeed surprising that the notched material subjected to long time tests shows pronouncedly brittle characteristics. This apparent discrepancy can, however, be bridged by taking the time-factor into account. The author has shown on a previous occasion that the original theory of equicohesive strength does not give full satisfaction as it does not include the influence of time as variable factor. In fact, only by including the time factor can order be created out of the chaos of the many apparently paradoxical observations.

Before applying the findings made on the tin-cadmium alloys to steels stressed at high temperature, it is essential to ascertain whether and to what extent the physical phenomena leading to the embrittlement of tin-cadmium alloy are encountered with steel also. This could be confirmed by a number of tests conducted on a 0.12 C—30.0 Ni—15 Cr steel containing small additions of W, Mo, and Ti, and another steel with 0.2 C—16 Cr—12 Ni, except for the fact that in the case of the steels some changes in structure may also take place.

Both notched and notch-free test bars of the 30 Ni—15 Cr were subjected to long time rupture tests, the material having been previously subjected to a stabilising heat treatment. These tests were conducted at 650 deg. C. The notch-free bars were of 10 mm. dia. and had a gauge length of 36 mm. The notched bars had a semi-circular notch of 2.5 mm. radius. The time-to-rupture values obtained are charted in Fig. 8 where the elongations (both with and without deformation) are also plotted. The test bar illustrated in Fig. 9 had been subjected to a stress of 23 kg. per sq. mm. fracture occurring after 31 hours ; while the bar illustrated in Fig. 10 was found to fail under 20 kg. per sq. mm. stress after 75¾ hours. With regard to the properties of this steel at 650 deg. C. it may be concluded that its cohesion strength is very poor, since the time-to-rupture stress curve of the notched bars intersects with that of the notch-free bars within the low time-to-rupture values shown. Also, in agreement with the observations made on the tin-cadmium alloys, the relation between elongation-with-deformation and deformation-less-elongation is very unfavourable, the former having a value of the order of 10 per cent and the latter of about 15 per cent. It may therefore be concluded that the creep of this steel under stress is almost exclusively due to grain-boundary plasticity. This hypothesis is fully confirmed by the appearance of the fractured bar, given in Fig. 10,

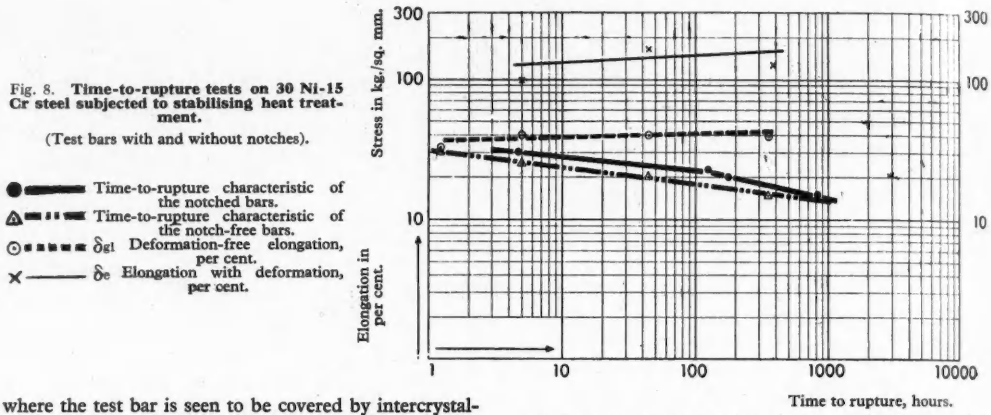

Fig. 8. **Time-to-rupture tests on 30 Ni-15 Cr steel subjected to stabilising heat treatment.**

(Test bars with and without notches).

where the test bar is seen to be covered by intercrystalline fissures. An attempt was made to improve the time-to-rupture strength by a heat treatment designed to increase structural stability, but with little success.

The strength characteristics of the 12 Ni—15 Cr material are charted in Fig. 11, in which the favourable relationship between elongation-with-deformation and deformation-less-elongation is a most notable feature. This material had been subjected to a special heat treatment producing an extremely stable structure. It is seen that the deformation-less-elongation ranges from 15-10 per cent, while the elongation-with deformation attains values between 150-90 per cent. This feature can be ascribed to an amorphous grain boundary plasticity. A bar which had failed under a stress of 25 kg. per sq. mm. after 44 hours is illustrated in Fig. 12. With a loading of 20 kg. per sq. mm., the material failed only after 432 hours, showing no traces of intercrystalline fissures.

Subsequent to these tests a piece of the same material was subjected to an additional heat treatment so chosen as to bring several constituents into supersaturated solution from which they could slowly precipitate at the test temperature of 650 deg. C. This precipitation then served to block the slip planes of the crystallites, at the same time enhancing the deformation process within the grain boundaries. As a direct result of this, the deformation-free-elongation was considerably increased and the elongation-with-defor-

Fig. 9. **30 Ni—15 Cr steel embrittled by heat treatment.** Stress 23 kg./sq. mm., time to rupture 23 hours. Magnification 7 ×

Fig. 10. **30 Ni—15 Cr steel, embrittled by heat treatment.** The same steel as Fig. 9, stress 20 kg./sq. mm., time to rupture, 75¾ hours. Magnification 7 ×

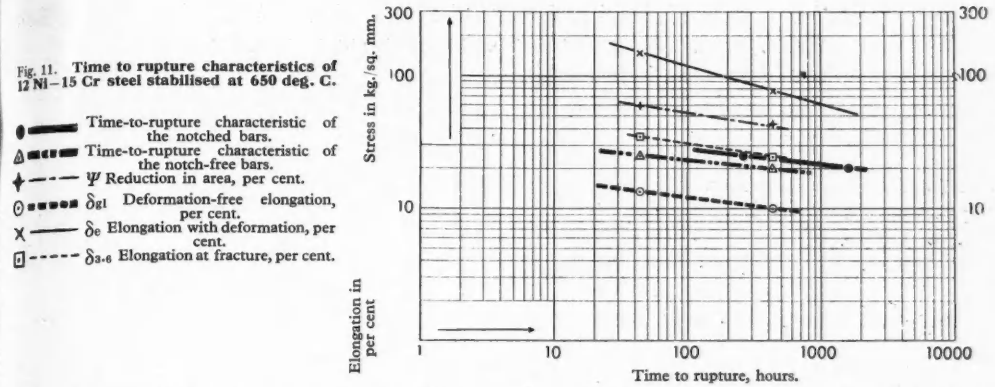

Fig. 11. Time to rupture characteristics of 12 Ni–15 Cr steel stabilised at 650 deg. C.

mation was decreased in the time-to-rupture test, which is to say, the material had become enbrittled because of the heat treatment applied, and its cohesive strength had decreased.

The effects produced by the action of triaxial stresses in the presence of notches are well illustrated by Fig. 13, the material being a heat resistant austenitic Cr-Mn steel. It will be noted that this bar had a weak spot at the bottom of the notch. This picture was taken after stressing the bar at 10 kg. per sq. mm. for 500 hours; it clearly shows the action of transversal stresses in the case of long time loading.

All these test results recorded with alloy steels go to show that the physical processes involved are identical with those observed in the case of the tin-cadmium alloys, excepting the presence of structural changes in the steel. From these findings it may be deduced that the mechanism of creep is qualitatively the same in every metal, and that intercrystalline fractures may happen in any metal. The main cause of such fractures is the precipitation of carbides, nitrides, or oxides, which causes a weakening of the grain boundaries accompanied by a simultaneous blocking of the slip planes in the crystals. It is known that precipitation processes as well as decomposition of austenite can be accelerated by cold working prior to application of the stress or by plastic deformation when the material is in the stressed condition. This explains why the diminution in cohesive strength is aggravated by the deformation attending the process of creep.

Short time test procedures based upon the observation of the creep rate during a certain interval of time cannot therefore be considered a suitable means for adjudging the high temperature qualities of a steel. On the basis of the experimental investigations described above, it would, however, appear quite feasible to develop a highly efficient short time test. This would consist in carrying out long-time-rupture tests on notched bars, contraction and elongation being measured in the usual manner. These data would then be used to establish both the deformation-less-elongation and the elongation-with-deformation, the ratio of the two being taken as a measure of the cohesive strength of the material. The superiority of the new method over previous practice seems to lie in the fact that emphasis is laid not so much upon ascertaining the absolute amount of elongation as upon the determination of the dangerous aspect of elongation originating from the amorphous plasticity of the grain boundaries.

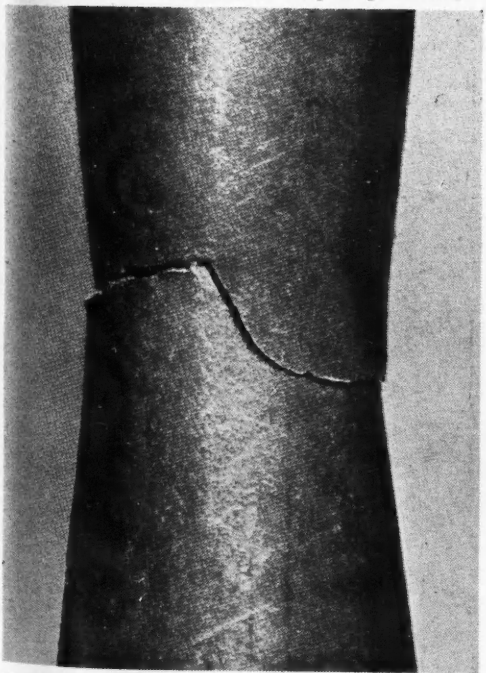

Fig. 12. 12 Ni–15 Cr steel, stabilised; loading 25 kg./sq. mm.; time to rupture 44 hours. Magnification 7 ×

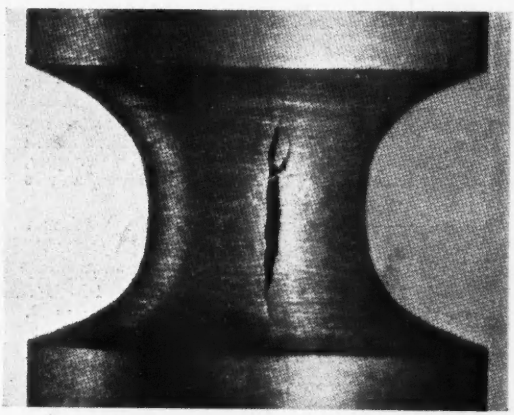

Fig. 13. Effect of transversal stress in notched test bar subjected to creep. Magnification 7 ×

X-RAY HIGH TENSION PLANT WITH RESONANCE TRANSFORMER.

By S. H. JENSEN. (From *Ingenioren*, No. 77, November 18, 1944, pp. 122-125.)

THE newly built X-ray laboratory at Copenhagen is equipped with a resonance transformer contained in a pressure vessel designed for 5 atm. internal pressure. This pressure vessel has a diameter of 1.70 m. and a height of 2.70 m. At atmospheric pressure flash-over takes place at 350 kV, but at four atmospheres pressure 850 kV can be carried with safety. The X-ray tube is seen to be arranged centrally within the pressure vessel (Fig. 1). It consists of 16 corrugated porcelain cylinders, the filament being arranged at the upper end of the tube. Vacuum is maintained by means of a set of vacuum pumps. Within the tube proper guidance of the electrons along the 2.5 m. long path between anode and cathode is ensured by means of a cylindrical focussing electrode located centrally within the porcelain tube.

The transformer itself constitutes a Tesla-coil, the secondary winding of which is wound around the X-ray tube. This secondary coil is 1.70 m. high and has a diameter of 55 cm. It is composed of 100 flat coils, each comprising 1600 turns. A view of the coil is given in Fig. 2. The coils which are stacked up one on top of the other are separated by distance pieces of bakelite, hereby securing an effective air circulation and cooling of the coil.

The primary coil is arranged below the lower end of the secondary coil. It has 75 windings, and is directly connected to a single phase alternator, the latter being driven by a direct current motor. The transformer core is so shaped that it envelopes the coil, thus forming a cylindrical shield vertically arranged within the pressure vessel. In magnetic respects this " core " is of little efficiency, except that it inhibits the generation of eddy currents in the pressure vessel. The resonance frequency of the transformer approximates to 300 cylces per second. Actual resonance is easily established by varying the speed of the d.c. motor driving the alternator, which has a frequency of 300 cycles at nominal speed. Up to 250 kV the tension prevailing at the terminals of the secondary coil has been measured by means of a spherical spark gap.

Simultaneous measurement of the current in the secondary coil has revealed an accurate proportionality between amperage and voltage, so that his relationship can be used to determine higher voltages by a simple extrapolation. As according to measurement 9 kV correspond to 1 mA, it follows from the relationship $V = I\,w\,L$ that $L = 3.2 \times 10^3$ Henry, and, as resonance will occur if $w^2LC = 1$, it is C = 55 cm.

As the magnetic circuit is not closed, the voltage distribution over the windings of the secondary coil is not uniform, but varies in the manner indicated in Fig. 3*a*. It is usual to use the expression $Q = \frac{\omega L}{R}$ as a criterion of the condition of sharpness of resonance. On the basis of the data applying to the coil in question it is found Q = 53. The value for Q can, however, also be determined from the resonance curve, and as $I = \frac{E}{R + j\left(\omega L - \frac{1}{\omega C}\right)}$ the current will attain a maximum if $\omega L = \frac{1}{\omega C}$ and it will decrease by $\omega L \div \frac{1}{\omega C} = R$. By introducing the difference $\omega_r - \omega_1$ where ω_r is the resonance frequency, it becomes $\omega L \div \frac{1}{\omega C} =$

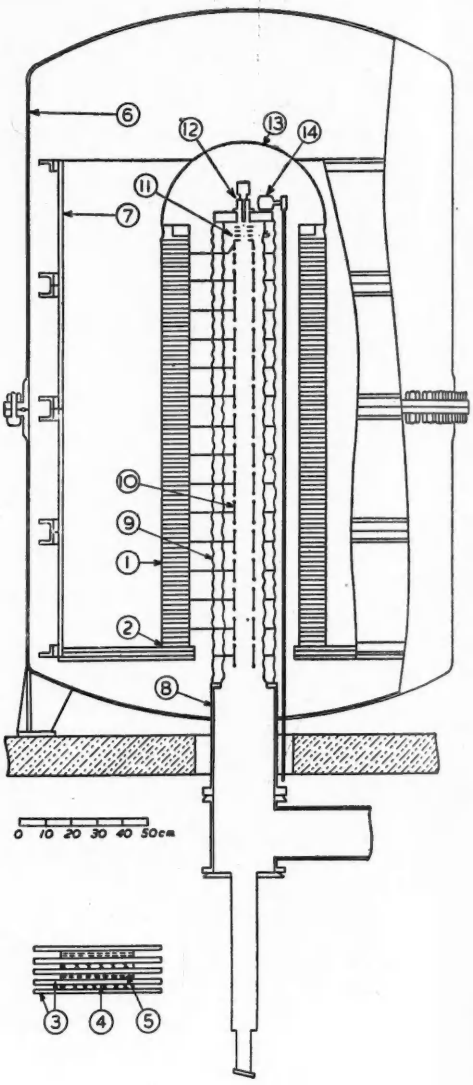

Fig. 1.

1. Secondary coil.
2. Primary coil.
3. Cardboard rings.
4. Winding.
5. Distance pieces.
6. Compressed air vessel.
7. Laminated iron shield.
8. X-ray tube socket.
9. Porcelain cylinder
10. Focussing electrode.
11. Top electrode.
12. Filament.
13. Corona screen.
14. Filament choke.

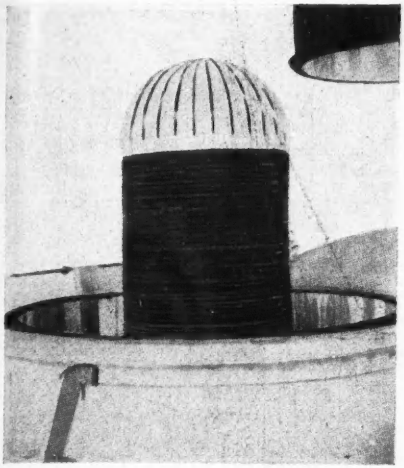

Fig. 2. **Top of secondary coil.**

$$= \frac{2\,\omega_r\,(\omega_r - \omega)}{\omega}\,.L = R,$$

so that

$$2.\ \frac{\omega_r\,.L}{R}\,.\,\frac{\omega_r - \omega}{\omega} = 1.$$

As it is $Q = \frac{\omega_r L}{R}$ it follows that $Q = \frac{\omega}{2\,(\omega_r - \omega)}$

Q is therefore determined by the width of the resonance curve at a height of 70.7 per cent of its maximum height. On this basis a value of Q = 22 obtains in the graph given in Fig. 3*b*.

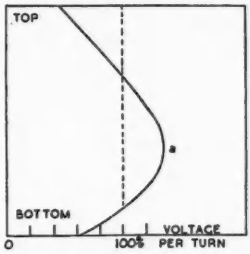

Fig. 3a. **Voltage distribution along secondary coil.**

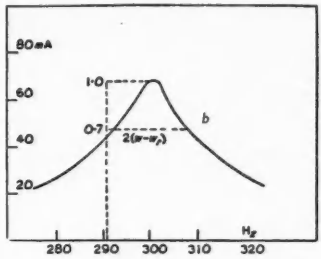

Fig. 3b. **Resonance curve (X-ray tube nut in operation).**

The considerable difference between the measured and the computed values for Q no doubt must be ascribed to various losses, in particular to the dielectric loss of the material used. Under prevailing conditions it was not, however, possible to secure an insulating material of better quality.

When operating the plant at 800 kV with a current output of 1.5 mA, the total power requirements amount to 6.5 KW, of which 2.7 KW are consumed by the motor-generator set.

IMPROVEMENT OF ENGINEERING CARBON STEEL.

By A. P. GULYAEV and F. M. HALPERIN. (From *Stal.*, Vol. 3, 1943, No.5/6, p. 49–51).

THIS report is concerned with the improvement of engineering carbon steel by the addition of small amounts of boron or of grainal. Several experimental heats were prepared in which deoxidation was carried out with the addition of boron, grainal, and aluminium respectively. The addition of boron was made in the form of chemically pure borax ($Na_2B\,O$) and manganese in the proportion of 95 per cent borax and 5 per cent manganese. The small addition of manganese was made for the purpose of activating the deoxidation process. The borax was pounded and then mixed with finely disintegrated manganese. The chemical analysis of the grainal was 61 per cent Fe, 11.33 per cent Al, 2.6 per cent Si, 2.6 per cent Ni, 6 per cent Ti, and 16.5 per cent V.

The heats were prepared in a high frequency furnace of 250 kg. capacity. Upon the addition of 300 grams of graphite powder and after deoxidation with 500 grams of ferrosilicon (corresponding to an addition of 2 kg. per ton), 125 grams of the special deoxidiser was added to the heat. The respective compositions of the three heats prepared were as follows :—

Deoxidised with	C	M	Si	P	S	Cr	Ni
A. Aluminium	0.45	0.39	0.46	0.036	0.026	0.15	traces
B. Boron ..	0.48	0.42	0.42	0.036	0.026	0.10	traces
C. Grainal ..	0.48	0.42	0.29	0.035	0.026	0.09	traces

The ingots were forged into rounds of 20, 30, and 55 mm. diameter respectively, their length varying from 380-400 mm. The forging temperature ranged from 1200-950 deg. C. Examination of the macro-structure of the forgings failed to reveal any porosity or other defects. After annealing at 850 deg. C. the forgings were machined. The finished rounds were water quenched from 850 deg. C. and then subjected to the Brinell hardness test. After that the pieces were tempered at 450, 500, 550 and 600 deg. C. respectively.

In order to determine the influence of the special deoxidiser upon the mechanical properties at various points of the cross section of the forgings, test bars were also taken from the core of the forgings. These bars were subjected to both tensile and impact tests. The brinell hardness of the impact test specimens was also ascertained. The test results are given in Fig. 1, where the mechanical properties of the three heats are charted as function of the diameter of the rounds.

A comparison of the different heats on the basis of an identical tempering temperature shows that the steels B and C have a tensile strength, and particularly a yield point much higher than steel A. This superiority of these two steels becomes still more pronounced in the case of large cross sections ; and it also increases with higher tempering temperatures. As the impact strength values show, the toughness of the three steels is substantially identical.

An examination of the structure of the various test bars (quenched from 850 deg. C. and tempered

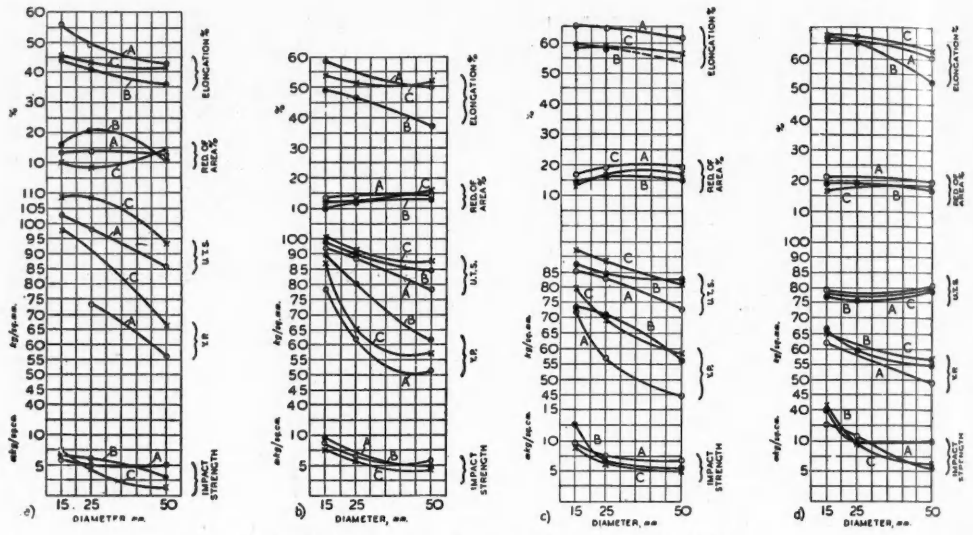

Fig. 1. **Mechanical properties versus diameter of the forging.**

Tempering temperature :
a : 450°C. b : 500°C. c : 550°C. d : 600°C.

at 550 deg. C.) showed that the 15 mm. dia. pieces were of sorbitic structure. The pieces of 50 mm. diameter showed pearlite in a ferrite network. The centre of the 25 mm. rounds of heat A showed pearlite and a small amount of ferrite. Steel B exhibited less ferrite than steel A, and steel C showed none. It can be concluded that in the case of the 25 mm. diameter rounds the desired improvement of the steel had been achieved as far as steels B and C are concerned. But steel C was not improved. All three steels showed a Rockwell hardness of 55-58 after quenching from 850 deg. C.

ANALYSIS OF SMALL MOTIONS BY MEANS OF THE PHOTO-ELECTRIC CELL.

By P. U. KNUDSEN. (From *Ingenioren*, 10th March, 1945 ; p. E22-26.)

PHOTOELECTRIC cells may be used for the study of small motions of relay armatures, contacts, and other devices, in which the movement ranges from a few millimeters to some hundredths of a millimeter. The diagram of the instrumentation for the investigation of the armature of a relay is given in Fig. 1. A beam of light is made to pass between the armature and the poles of the electromagnet and subsequently to strike the photo-electric cell. The cell current is passed to an amplifier, the latter in turn energizing the cathode ray oscillo-graph. An interruptor device is employed for sending synchronous impulses at the rate of 5-10 impulses per sec. to both the relay coil and the deflector coil of the oscillograph, thus producing a stationary image on the screen of the cathode ray tube. The time basis can be adjusted to give the image of the beam of rays a fixed velocity, as e.g. 1 millimeter per millisecond.

The photoelectric cell is a caesium-vacuum cell. The specially designed amplifier is of the two-stage direct current type and is so arranged that it can also be used for making static measurements. Each valve has its own current supply, and the supply voltage of the first stage valve is stabilised by means of a neon glow lamp. Both cathode ray and moving-coil type oscillo-graphs may be used in conjunction with the amplifier, the maximum output of which is 75 mA.

The first apparatus of this type was equipped with an interruptor of the relay type, but a rotary interruptor is now available with a maximum speed of 25 revolutions per second, corresponding to the speed of telegraph relays. The speed of the time basis device can be adjusted in steps, so that 1 cm. can be made equivalent to 10, 5, 2, or 1 ms. etc.

An oscillogram of a relay with one contact point obtained with the use of a moving-coil type oscillograph is shown in Fig. 2. The bottom curve represents the

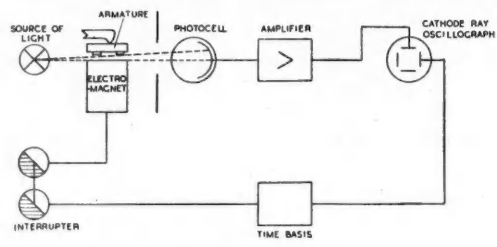

Fig. 1.

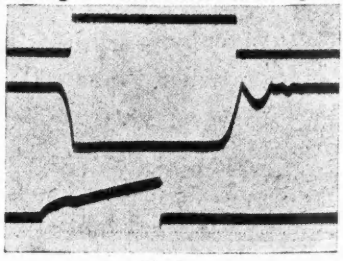

Fig. 2.

current passing through the relay coil, the hump in the ascending part of the curve being due to the movement of the armature. The motion of the armature is given by the curve above the current characteristic. The length of travel of the armature amounts to 0.47 mm. It is seen that the armature remains at rest for 7 milliseconds after closure of the coil circuit, until the magnetic field has attained sufficient strength to set the armature in motion. After a further 6 milliseconds the contact is closed, as will be seen from the topmost curve of the oscillogram. It will also be seen that because of the prevailing remanence the armature does not fall off for 30 milliseconds after the coil current has been interrupted. The movement of the armature of a relay with 12 contacts is recorded in Fig. 3. Here the armature is seen not to move until 13 milliseconds after closing of the relay coil circuit; after a further 18 milliseconds the contacts are closed. The oscillogram of the armature movement shows that the motion

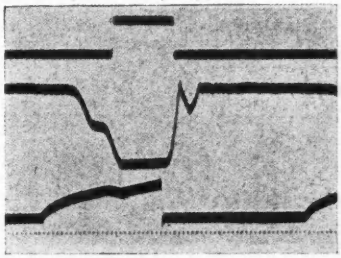

Fig. 3.

is temporarily arrested at the point of travel where the counterthrust of the contact springs has to be overcome.

THE JALBERT SYSTEM OF AIR BLAST INJECTION

(From *Le Génie Civil*, Vol. 121, 1944; No. 19/20, pp. 154–55.)

THE volatility of ethyl alcohol is considerably less than that of petrol, and in addition to this the latent heat of evaporation of alcohol amounts to 206 cal. as compared to 74 cal. in the case of petrol. The volatilisation of alcohol in a carburettor designed for petrol cannot therefore be carried out except by special measures. Even so, a suitably modified carburettor is not very reliable in service, particularly in the cold season. But these drawbacks may be avoided by the mechanical injection of the fuel into the cylinder. This method ensures that the correct amount of fuel required for optimum operating efficiency is supplied to the cylinder, and this irrespective of atmospheric conditions.

The Jalbert air blast injection system is especially designed for the purpose of enabling the alternative running of an internal combustion engine on ethyl alcohol, methyl alcohol, or heavy oil. The injection system developed is outlined in Figs. 1 and 2, which show details of a four-stroke cycle engine. The cylinder is connected with a special injection cylinder (b) containing a piston (c). The big end of the pistion rod (d) of the piston is carried on the crank (e) of the overhead shaft (f) revolving at half the engine speed. Injection into the engine cylinder takes place through the automatic valve (g) loaded by the valve spring (h). The mixture to be injected is passed from the injection cylinder (b) to the valve by way of the passages (i). When the piston (c) reaches the top dead centre position, a lateral port (j) is uncovered in the cylinder wall through which mixture is aspirated from the carburettor (k). The latter is adjusted to deliver a rich mixture. While its composition is calculated to ensure complete combustion in the engine cylinder, its richness is too high to cause ignition in the injection cylinder when compression and discharge into the engine cylinder takes place on the downward stroke of piston (c).

Subdivision of the injection process into two phases is obtained in the following manner: If P and p are the respective pressures in kg./sq. cm. in injection cylinder and engine cylinder, R the pull in kg. of the valve spring; and if S and s are the sectional areas of the valve on the injection cylinder side and the engine cylinder side respectively, then the opening force acting upon the valve will be P.S and the closing force will be pS+R. The respective pressures prevailing in the injection cylinder and in the engine cylinder are charted in Fig. 3 as functions of the crank angle, and it will be seen that the engine cylinder pressure continuously increases during the compression stroke of the piston. The compression in the injection cylinder takes place between —80 and + 180 deg. crank angularity and would be represented by the curve ABCD if the injection valve were blocked in the closed position. Actually, however, the closing force exerted by the valve spring (h) will be overcome by the injection cylinder pressure at the point (C), which results in a first injection, the angle α being determined from the relationship $P_\alpha\ s = P_\alpha\ S + R$.

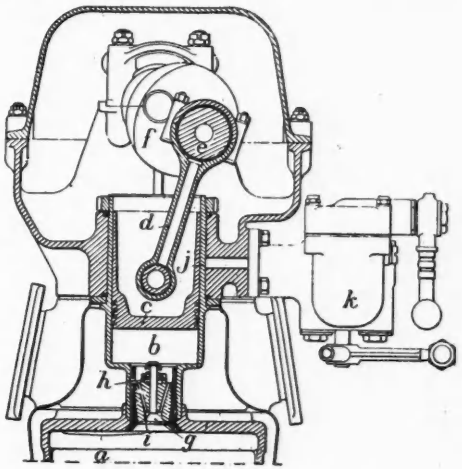

Fig. 1. **Jalbert injection system.**

(a) T.D.C. position of engine piston.
(b) Injection cylinder.
(c) Piston of injection cylinder.
(d) Connecting rod.
(e) Crank.
(f) Overhead shaft.
(g) Automatic valve.
(h) Spring.
(i) Passages.
(j) Admission port.
(k) Carburettor.

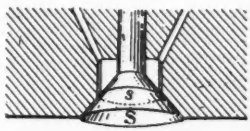

Fig. 2. **Detail of admission valve.**

The pressure prevailing in the engine cylinder will not be materially affected by the injection, as the volume of the engine cylinder is much greater than that of the injection cylinder. The pressure in the latter will, however, sharply decrease at the moment of injection and will therefore proceed along line CE in the diagram; it will then again increase along the adiabatic curve EFG.

At point F corresponding to a crank β it will be

$$P\beta\ s = p\beta\ S + R$$

so that the injection valve will open once more and discharge a second injection into the engine cylinder. The relative cylinder volumes as well as size of the the injection valve and the thrust of the valve spring are so chosen that the two injections take place at 75 deg. and 155 deg. crank angle respectively. It can be computed that the total weight of mixture introduced into the engine cylinder during the two injections amounts to 56 per cent of the amount of mixture originally aspirated by the injection cylinder. Sixty per cent of the total amount injected into the engine cylinder is accounted for by the first injection, and 40 per cent by the second injection. Thus, 60 per cent of the total fuel required per working cycle is injected at a crank angle 110 deg. in advance of the top dead centre position. This affords sufficient time for intimate mixing without causing any danger of ignition. At the end of this first injection period the concentration of mixture in the combustion space of the cylinder amounts to only 3.75 per cent of the weight of the air; while a figure of 6.25 per cent, equally 1 g. of combustible for ever 15 g. of air present, is required to create maximum inflammability. On the other hand the concentration of combustible in the mixture contained in the injection cylinder amounts to 78 per cent, which is much too high to permit spontaneous ignition. These conditions persist throughout the interval between the crank positions of 70 and 155 deg. The latter position marks the commencement of the second injection of mixture into the engine cylinder. But this time the injection causes spontaneous ignition as the injected mixtures diffuses into the hot air contained in the cylinder space. The temperature of combustion attained will exceed that recorded with heavy fuels. This is due to the smaller amount of heat required for vaporisation.

The fuel supply to the engine cylinder per working cycle may be varied either by changing the richness of the aspirated mixture or by changing the quantity of the mixture supplied. The modification of the richness of the mixture aspirated by the injection cylinder is effected by varying the amount of mixture aspirated from the carburettor; while the amount of air aspirated is left unchanged. The injection characteristics obtaining with this mode of operation are substantially identical with the characteristic curves given in Fig. 3.

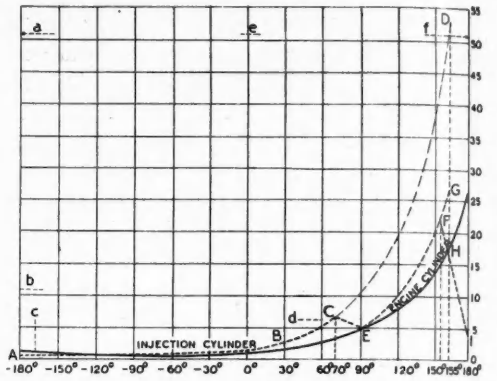

Fig. 3. **Pressure diagrams for engine cylinder and injection cylinder respectively.**

If the fuel supply is controlled by varying the quantity of the mixture supplied to the engine cylinder, different characteristics will obtain, since the pressure rise characteristic of the injection cylinder will now be lower owing to the smaller amount of mixture aspirated. Consequently, injections will occur at a later stage. This method of engine output control is, however, less frequently resorted to.

A "multi-fuel" engine embodying the Jalbert injection system has been built by the Société des Atéliers et Chantiers de la Loire. This is a 16 cylinder H-type engine of 130 mm. dia. bore and 130 mm. stroke developing 600 h.p. at a speed of 2,550 r.p.m. The weight of this engine is 570 kg. and its specific fuel consumption amounts to 175 grams of gas oil per h.p. hour. This engine was built for aviation purposes and was tested by the French Air Ministry prior to the war. After the war a rail-car engine with 12 cylinders arranged in line was designed. This engine is now under construction. An experimental single cylinder research engine was built and was run on various fuels ranging from gas oil to petrol. The tests conducted so far have shown that the Jalbert injection system yields an m.e.p. of 8 kg. per sq. mm., and this without resorting to supercharging, the engine speed approximating to 3000 r.p.m.

THE HEATING OF WIRE IN WIRE DRAWING

By E. SIEBEL and R. KOBITZSCH. (From *Stahl und Eisen*, Vol. 63, No. 6, 1943, pp. 110-113).

WHEN drawing wire at high speed considerable heating of the wire and die can be observed which necessitates cooling of the die. The temperature in the die at speeds above 2 metre/sec. is about 200 to 300 deg. C. for steel wire, while the temperature of the drawn wire on reeling is about 100 deg. C. As the thickness of the lubricating film between wire and die can only be very small, there must be a very great temperature gradient in the surface layers of the wire which drops suddenly behind the die.

HEATING OF WIRE DUE TO STRAIN ENERGY.

The temperature distribution in the wire in passing the die can be estimated with sufficient accuracy. It is necessary to assume that both the strain energy and the energy due to friction are transformed into heat. The strain energy per unit volume is $k_{fm} \cdot \varphi_h$, where k_{fm} is the mean strength value in drawing and φ_h the deformation of the wire in pressing the die. In the wire axis $\varphi_h = \log_e \frac{F_o}{F}$, when F_o is the original wire cross section, and F is the cross-section of the die. In the surface layers, additional flow increases the deformation.

The deformation leads to an increase in temperature

$$t_1 = \frac{\varphi_h \cdot k_{fm}}{A \cdot c \cdot \gamma} \quad .. \quad .. \quad .. \quad (1)$$

where $A = 427$ mkg./kcal. is the mechanical equivalent of heat, c the specific heat and γ the weight per unit volume of the wire.

HEATING OF WIRE DUE TO FRICTION.

The work expended in drawing wire produces heat that partly goes into the wire, partly into the die. The

heat produced in the boundary layer between wire and die is expressed as

$$\frac{dq}{dz} = \frac{\mu \cdot k_{fm} \cdot v}{A} \quad .. \quad .. \quad (2)$$

Herein, $\mu\, k_{fm}$ is the frictional force per unit area, v the speed of drawing.

Let us consider first the limiting case by putting the thermal conductivity of the die equal to zero. As the whole frictional heat then passes into the wire, there must be at the surface of the wire a temperature gradient

$$\frac{dt}{dx} = \frac{1}{\lambda} \cdot \frac{dq}{dz} = \frac{\mu \cdot k_{fm} \cdot v}{A \cdot \lambda} \quad .. \quad .. \quad (3)$$

where λ is the conductivity of the wire. Accordingly, the temperature increase in the surface layer of the wire be t_a. Assuming that the thickness of the heated layer is b at a distance of unity from the die entry, and that there is a parabolic temperature distribution according to Fig. 1, the temperature increase at a distance $(b-x)$ from the surface is

$$t_x = \frac{1}{\lambda} \cdot \frac{dq}{dz} \cdot \frac{x^2}{2b} = \frac{\mu \cdot k_{fm} \cdot v}{A \cdot \lambda} \cdot \frac{x^2}{2b} \quad .. \quad (4)$$

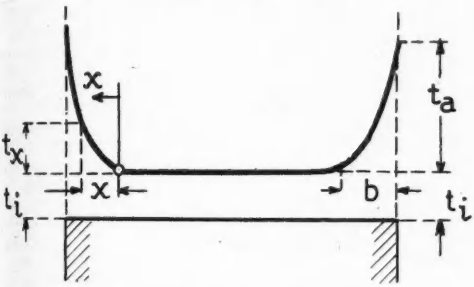

Fig. 1. **Temperature distribution across the wire section**

The total heat of this layer per unit area is given by

$$q = \int_0^b t_x \cdot dx \cdot c \cdot \gamma = \frac{\mu \cdot k_{fm} \cdot v}{A\,\lambda} \cdot c \cdot \gamma \cdot \frac{b^2}{6} \quad .. \quad (5)$$

This must equal the amount of heat pressing into the wire over a length l per unit area, i.e.,

$$q = \frac{\mu\, k_{fm} \cdot l}{A} \quad .. \quad .. \quad (6)$$

Thus,

$$\frac{\mu \cdot k_{fm} \cdot v}{A\,\lambda} \cdot c \cdot \gamma \cdot \frac{b^2}{6} = \frac{\mu \cdot k_{fm} \cdot l}{A},$$

and the thickness of the layer

$$b = \sqrt{6 \cdot \frac{l}{v} \cdot \frac{\lambda}{c \cdot \gamma}} = 2.44 \sqrt{\frac{l}{v} \cdot \frac{\lambda}{c \cdot \gamma}} = 2.44 \sqrt{\frac{\lambda}{c \cdot \gamma} \cdot z} \quad (7)$$

Substituting equation (7) into equation (4), we have

$$t_a = \frac{\mu \cdot k_{fm} \cdot v}{A \cdot \lambda} \cdot \frac{b}{2} = 1.22 \frac{\mu \cdot k_{fm}}{A} \sqrt{\frac{l \cdot v}{\lambda \cdot c \cdot \gamma}} =$$

$$= 1.22 \frac{\mu \cdot k_{fm} \cdot v}{A} \sqrt{\frac{z}{\lambda \cdot c \cdot \gamma}} \quad .. \quad .. \quad (8)$$

Taking heat conductivity of the die into account, part of the heat due to friction (q) presses into the wire ($q' = m.q$) the other part goes into the die ($q'' = nq$). Therefore,

$$q = q' + q'' = m\,q + n\,q \quad .. \quad .. \quad (9)$$

and equation (3) assumes the form:

$$\frac{dt}{dx} = m \cdot \frac{\mu \cdot k_{fm} \cdot v}{A \cdot \lambda} \quad .. \quad .. \quad .. \quad (3a)$$

where m at die entry always <1, at die exit possibly >1.

The temperature increase at the wire surface can now be obtained from equations (1) and (8).

$$t = t_1 + t_a = \frac{\varphi_h \cdot k_{fm}}{A \cdot c \cdot \gamma} + 1.22\, m \cdot \frac{\mu \cdot k_{fm}}{A} \cdot \sqrt{\frac{l \cdot v}{\lambda \cdot c \cdot \gamma}} \quad (10)$$

Substituting for $A = 42700$ cm. kg./cal., we have

$$t = 2.35 \times 10^{-5} \times k_{fm} \left(\frac{\varphi_h}{c \cdot \gamma} + 1.22\, m\mu \sqrt{\frac{l\,v}{\lambda\, c\, \gamma}} \right) \quad (10a)$$

An example will show the magnitude of the temperature increase at the wire surface. Let us assume steel wire drawn at a speed $v = 100$ cm./sec. through a die of $d_o = 0.5$ cm., $d_1 = 0.4$ cm. and $d_m = 0.45$ cm. The deformation be $\varphi_h = 0.44$, at an inclination $\sin \alpha = 0.1$, i.e., $l = 5$ mm. The material is defined by:

mean strength in drawing .. $k_{fm} = 5000$ kg./cm²
weight per unit volume .. $\gamma = 7.8 \times 10^{-3}$ kg./cm³.
specific heat .. $c = 0.115$ kcal./kg. deg. C.
heat conductivity .. $\lambda = 45$ kcal./m. hr. deg. C.
$= 0.125 \times 10^{-3}$ kcal./cm. sec., deg. C.

Substituting these values together with assumed values $\mu = 0.05$ and $m = 0.8$ into equation (10a) we obtain $t_1 = 58$ deg. C., and $t_a = 118$ deg. C.

Thus, the total temperature increase at the surface is

$$t = t_1 + t_a = 58 + 118 = 176 \text{ deg. C.}$$

The thickness of the layer influenced by frictional heat is calculated by equation (7) to $b = 0.65$ mm. An increase of the drawing speed to $v = 200$ cm./sec. would increase the surface temperature to $58 + 166 = 224$ deg. C., while the thickness b would decrease to 0.45 mm.

THE WIRE TEMPERATURE AFTER PASSING THE DIE.

As soon as the wire passed the die all external heat input ceases. Accordingly, the temperature gradient at the wire surface becomes zero.

The stored heat in the surface layer of the wire flows towards the wire interior until the temperature is constant through the cross-section. The temperature increase t_{am} due to frictional heat after the temperature levelling has taken place can be expressed as

$$t_{am} = \frac{2}{R^2} \int_0^R x \cdot t_x \cdot dx = \frac{1}{6}\, t_{(x=R)} \cdot \frac{R-r}{R} \left(3 + \frac{r}{R} \right) \quad (11)$$

$t_{(x=R)} = t_a$ denotes the temperature increase due to frictional heat on the wire surface at the die exit, and t_x the temperature increase at distance x from the wire axis, while $r = R - b$.

Applying this to the above given example, the temperature peak on the wire surface drops to half of its value 3 mm. behind the die, i.e., in 0.003 seconds. The mean temperature increase in the wire when constant temperature level has been reached, calculated by equation (11) yields $t_{am} = 24$ deg. C.

CONSEQUENCES OF THE HEATING OF THE WIRE.

The high temperatures at great drawing speeds which occur in the surface layer have great influence on the lubrication, as viscosity decreases with increasing temperature. Conditions for small diameters are here more advantageous than for large ones.

The non-uniform heating of the wire cross-section is responsible for tensile stresses in the outer layers and

compressive stresses towards the core. The magnitude of these stresses is given by the following equation

$$\sigma_l = \frac{E}{1-\gamma} \cdot \alpha_t \cdot (t_a - t_{am}) \quad .. \quad (12)$$

Herein, E is Young's modulus and α_t the thermal coefficient of expansion of the wire material. For steel $E = 20{,}000$ kg./mm². and $\alpha_t = 1.2 \times 10^{-5}$ mm./mm. deg. C. With $t_a - t_{am} = 118 - 24 = 94$ deg. C., the tensile stress in the outer layer becomes

$$\sigma_{l_1} = \frac{20000}{1-0.3} \times 1.2 \times 10^{-5} \times 94 = 32 \text{ kg./mm}^2,$$

while the compressive stress in the core is

$$\sigma_{l_2} = -\frac{20000}{1-0.3} \times 1.2 \times 10^{-5} \times 24 = 8 \text{ kg./mm}^2.$$

This implies the advantage of reduction in drawing speed in the last stage of drawing.

JET PROPULSION PROBLEMS

By A. MÖRTSELL and S. E. NORBERG. (From *Teknisk Tidskrift*, Vol. 74, 1944, pp. 871-878).

REACTION-TYPE or jet propulsion plants may be classified according to whether they are of the pulsating or of the continuous discharge type. Both types may operate at either high or low pressure, provided air and volatile or gaseous fuel are used. Low operating pressure requires the employment of relatively large propulsion plant components. On the other hand, operation at high working pressure involves greater practical difficulties. The employment of a pulsating discharge requires heavier plant components, but at the same time thermal operating conditions are less severe.

An explosion type jet propulsion system could be visualised in the shape of an internal combustion engine arranged for partial expansion. The final expansion would be effected in the jet propulsion by discharging the exhaust gases through the jet nozzle with high velocity. It would, however, be difficult to determine at which point expansion in the engine should terminate in order to obtain highest overall efficiency of the system. In order to gain some information as to how much of the energy supplied to the engine can be utilised in the form of jet or reaction energy, it may be assumed that 80 per cent of the effective work of the engine is to be converted into reaction energy, the remaining 20 per cent to cover compression and mechanical losses. Further assuming a thermal efficiency of 30 per cent based on operation on the conventional diesel cycle, there would be available for jet propulsion $3 \times 8 = 24$ per cent plus the normal exhaust loss of 30 per cent, that is, a total of 54 per cent of the calorific value of the fuel. To convert this 54 per cent into jet energy would, however, be difficult, particularly in view of the considerable losses to be expected in both the engine exhaust valve and the jet propulsion nozzle.

Four different types of jet propulsion systems will be investigated, all of which are of the constant pressure combustion type, the combustion air being brought up to combustion chamber pressure by means of a centrifugal or axial-flow compressor of a suitable design.

The first of these systems is outlined in Fig. 1. Here an internal combustion engine is employed to drive the compressor, from whence the air is supplied to the combustion chamber via a receiver. Assuming, for instance, that in a small system of this kind some 20

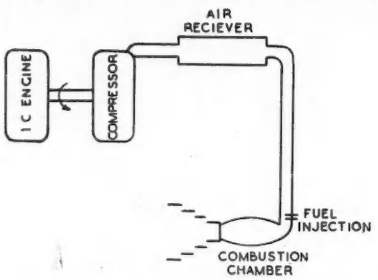

Fig. 1. **Diagram of propulsion system, No. 1.**

cu.m. of air per hour are to be compressed from atmospheric pressure to 20 atm., the theoretical power consumption will approximate to some 2.5 h.p. Actually, a 4.4 h.p. engine will be called for with a theoretical heat rate of some 2,800 kcal. per hr., and a fuel consumption of 1.13 kg. per hour. The weight of the jet gas will be the weight of 20 cu.m. of air at atmospheric pressure equal to 23 kg. plus the weight of the fuel supplied to the combustion chamber, which weight may be taken as 1.6 kg. per hour.

The total fuel consumption will thus be 2.73 kg. per hour, of which 41 per cent is consumed by the compressor drive and 59 per cent is used in the combustion chamber. The total heat requirements are then found as $2.73 \times 11{,}000 = 30{,}000$ kcal. per hour. With a thermal engine efficiency of 23 per cent, 0.23×41 per cent, that is, 9.5 per cent of the total heat supply, will be available as useful output. As the work of adiabatic compression theoretically amounts to 2.5 h.p., the sensible heat content of the air supplied to the combustion chamber will at most be $\frac{2.5}{4.4} \times 100 = 57$ per cent of 9.5 per cent, that is, 5.5 per cent.

Since 1.6 kg. of fuel, equal to 17,600 kcal. (or 59 per cent of the total heat consumption) are introduced into the combustion chamber, the total heat supply to the latter will be $5.5 + 59 = 64.5$ per cent of the total heat consumption of the propulsion plant as a whole. Assuming the thermal and friction losses in the combustion chamber as 40 per cent, the jet energy available will be $0.6 \times 64.5 = 38.7$ per cent of the total heat supply. The jet energy is therefore equivalent to $38.7 \times 30{,}000 = 11{,}600$ kcal. per hr. $= 18.1$ h.p. The theoretical velocity of the discharge, that is, the jet velocity, is given by

$$\frac{Q.w^2}{g \cdot 2} \cdot \frac{1}{75} = \frac{23 \cdot w^2}{3{,}600 \cdot 9.81 \cdot 75.2} = 18.3 \text{ h.p.}$$

so that $w \cong 2{,}000$ m./sec. where $Q = \frac{23}{3600}$ is the quantity of gas discharged in kg. per second.

But this gas quantity is too small to give a sufficiently large jet action for the purpose under consideration. Therefore, in order to increase the reaction force, the energy available in the combustion chamber must be imparted to a larger mass of gas. This required addition of air can be carried out by ejector action. If, for instance, the force of reaction is to be increased fifty fold, it will be $\frac{m w^2}{2} = L$ and $m \cdot w = P$, where P is the force of reaction. For 50 P it is $m_1 w_1 = 50 P$, that is $w_1 = \frac{50 P}{m_1}$, and it is also $\frac{m_1 w^2_1}{2} = L$; henceforth $m_1 = 2500 m$ and $50 w_1 = w$.

This goes to show that the air quantity must be increased 2500 times if the force of reaction is to be

increased 50 times. At the same time the gas velocity is decreased to one-fiftieth of its original value. The overall efficiency of the jet propulsion plant and its effective power output will vary with both the air pressure and the combustion chamber losses, as enumerated in Table I, and charted in Figs. 2 and 3.

The overall efficiency of the jet propulsion plant will, however, also depend on the efficiency with which the energy of the jet can be utilised. The compressor drive and the compressor proper of a reasonably large aircraft propulsion plant of this type will each have a unit

TABLE I.

Compulsion chamber losses per cent	Overall efficiency per cent			Propulsion effect h.p.		
	Air pressure, kg./cm2.					
	20	10	5	20	10	5
0	64,5	72,2	80	30,5	29,5	29,0
40	38,7	43,3	48	18,3	17,6	17,4
60	26,0	29,0	32	12,3	11,9	11,6
80	13,0	14,5	16	6,15	5,95	5,8
90	6,5	7,2	8	3,07	2,95	2,9

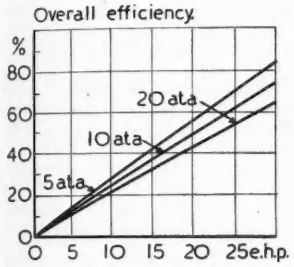

Fig. 2. **Interrelationship between overall efficiency of propulsion plant and plant capacity for different air pressures.**

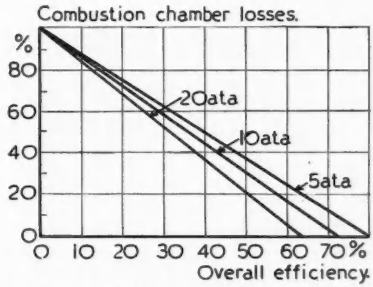

Fig. 3. **Influence of combustion chamber losses upon propulsion plant efficiency for different air pressures.**

weight of 0.8 kg. per h.p.; while the combined weights of auxiliary plant and combustion chamber will be some 200 kg. For a proposed plant to develop a reactive force of 1000 h.p., the salient data are tabulated in Table II, and the total fuel consumption data are charted in Fig. 4. It will be noted that these data are established on the assumption of three different combustion chamber pressures.

In the jet propulsion system outlined in Fig. 5, a portion of the jet energy is used to operate the gas turbine which serves as compressor drive. The third type of jet propulsion plant examined is diagrammatically shown in Fig. 6. In this layout the internal combustion engine which drives a low pressure air compressor is made as large as possible. The efficiency of the internal combustion engine may be taken as 30 per cent, and that of the compressor as 70 per cent.

For a jet propulsion unit developing a useful power of 1000 h.p. an engine of at least 1430 h.p. would be required, assuming $F=0$. Taking the unit weight of the engine as 0.8 kg. per h.p. and that of the compressor as 0.6 kg. per h.p., their combined weight will be

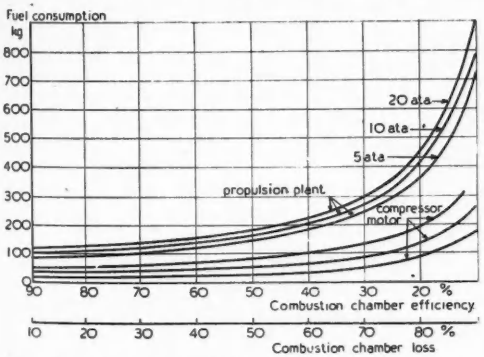

Fig. 4. **Spec. fuel rate of 1,000 h.p. propulsion plant for different air pressures.**

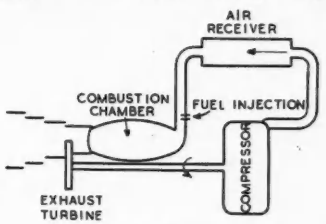

Fig. 5. **Diagram of propulsion system No. 2.**

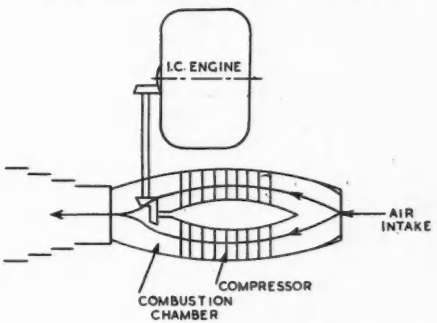

Fig. 6. **Diagram of propulsion system No. 3.**

TABLE II.

Compulsion chamber losses per cent	Compressor drive h.p.			Total weight of plant kg.			Total fuel rate kg./h.			Fuel rate of compressor drive kg./h.		
	Compressed air pressure, kg./cm2.											
	20	10	5	20	10	5	20	10	5	20	10	5
0	147	102	65,5	436	364	305	—	80	72	37,8	26,2	16,8
40	238	171	109	580	472	374	149	133	120	61	44	28
60	380	252	163	810	640	462	222	200	180	98	65	42
80	720	500	330	1 354	1 000	728	443	400	360	185	129	85
90	—	1 020	660	—	1 840	1 260	890	800	720	—	260	170

1900 kg. To this 200 kg. will have to be added to cover the weight of the combustion chamber, air intake and ducting, etc. The total weight of the propulsion plant would therefore amount to some 2,100 kg., which is equivalent to a unit weight of 2.1 kg. per h.p. If the unit weights of compressor and compressor drive are taken as 0.5 kg. per h.p., the unit weight of the propulsion plant will amount to 1.63 kg. per h.p. The specific fuel rate of a propulsion plant of this type will exceed the specific fuel consumption of an engine-air-screw type of plant by at least 43 per cent.

The fourth type of jet propulsion system may be represented by any possible combination of the three aforementioned systems. In cases where the fuel/air mixture in the combustion chamber would become insufficient to maintain stable combustion, the employment of a special burner of the Bunsen type having its own air supply might be considered.

While systems No. 1 and 2 appear to be the most promising, it is impossible to state in general terms which one of the various systems is really the best. Thus system No. 2 looks particularly attractive in principle, but at the present stage of development the design of the gas turbine may prove a most formidable task. Moreover, this system would require a larger combustion chamber than system No. 1, as it has to deal with the entire fuel supply to the system. A possible modification of system No. 2 would consist in the provision of a separate combustion chamber for the turbine, as outlined in Fig. 7. It appears not unlikely that both from the aspects of overall efficiency and unit weight this hook-up may prove the most attractive; but its development is naturally bound up with further advances in gas turbine technique.

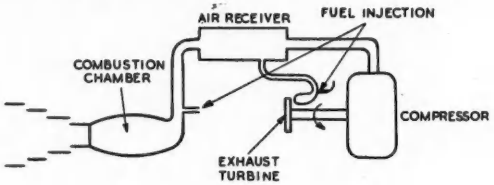

Fig. 7. Diagram of modified propulsion system No. 3.

From the aspect of high altitude flying, systems No. 1 and 2 should prove superior to the conventional I.C. engine-propeller drive, provided that a satisfactory overall efficiency can be achieved. For the purpose of high altitude flying, the I.C. engine which drives the compressor could be overdimensioned and equipped with either an ordinary or a gas turbine driven supercharger to operate only at fractional load. Its full capacity would, however, be momentarily available also for starting and climbing, and this would be achieved with the use of an engine of relatively low weight, representing about 30 per cent of the weight of the jet propulsion plant as a whole. Similar high altitude characteristics could be obtained with the modified system 2 shown in Fig. 7.

In the case of system 4, and particularly of system 3, it would be more difficult to arrange the propulsion plant for altitude flight than with the present day engine-propeller system.

The force of impulse is $P_1 = m \cdot w$, where w is the gas velocity in m./sec. relative to the aircraft, and m is the mass of gas expelled in kgs²/m. P_1 is thus seen to be unaffected by the speed of the aircraft. The *total* propelling force P acting upon the plane must, however, be smaller than P_1, as the travelling speed v of the aircraft must be imparted to the mass of air m which is introduced into the jet propulsion plant. This mass of air acts as a brake, the braking force amounting to $P_2 = m \cdot v$. The total effective propulsive force is therefore given by $P = m\,(w - v)$, and the useful energy output or propulsive effect is expressed by $N_1 = m \cdot v\,(w - v)$. The energy supplied to the air, as it passes through the jet propulsion plant, is given by the difference in the kinetic energy of the air at inlet and outlet respectively, that is to say,

$$\frac{m \cdot w^2}{2} - \frac{m \cdot v^2}{2} = N_2.$$

The efficiency of the jet propulsion plant is then given by

$$\eta = \frac{v\,(w - v)}{\frac{w^2}{2} - \frac{v^2}{2}} = \frac{2v}{w + v}$$

This expression for the efficiency can also be arrived at by viewing the expelled mass of gas from the ground. In this case the speed of the jet will be expressed by $(w - v)$ and its kinetic energy will amount to $m\frac{(w-v)^2}{2}$, which from the aspect of propulsion must be considered a total loss. The energy consumption was found above as $N_2 = \frac{m\,w^2}{2} - \frac{m\,v^2}{2}$, while the energy actually utilised is $\frac{m \cdot w^2}{2} - \frac{m \cdot v^2}{2} - m\frac{(w-v)^2}{2}$ $- m \cdot w \cdot v - m\,v^2$. The efficiency is therefore again given by:

$$\eta = \frac{m \cdot w \cdot v - m \cdot v^2}{\frac{m \cdot w^2}{2} - \frac{m \cdot v^2}{2}} = \frac{2v}{w+v}$$

By dividing both numerator and denominator by w, it becomes

$$\eta = \frac{\frac{2v}{w}}{1 + \frac{v}{w}}$$

which is represented by curve (1) in Fig. 8.

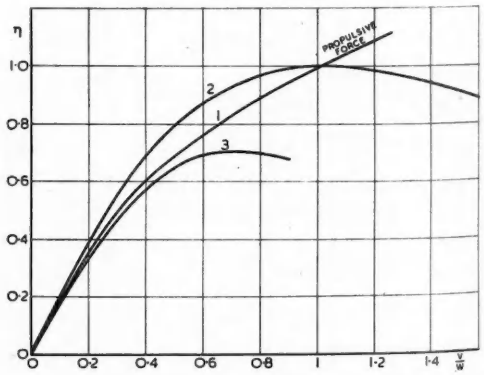

Fig. 8. Efficiency characteristics of jet propulsion and rocket plants.

Rocket Drive.

In the case of a rocket drive, the propulsive efficiency will be given by

$$\eta = \frac{2 - \frac{v}{w}}{1 + \left(\frac{v}{w}\right)^2}$$

when the rocket is in flight (curve (2) in Fig. 8) and

$$\eta = \frac{2 - \frac{v}{w}}{1 + 2\left(\frac{v}{w}\right)^2}$$

if the period of acceleration is included (curve (3) in Fig. 8).

Thermodynamics of Jet Propulsion.

An investigation of the thermodynamic characteristics of the jet propulsion plant meets with the difficulty of estimating the losses by radiation and conduction, as well as by friction. In order to avoid the necessity of establishing excessively complicated analytical expressions the problem will be treated in the following simplified manner.

The combustion air may be assumed to undergo adiabatic compression, followed by the supply of heat at constant pressure. Expansion is then carried out adiabatically, as indicated by the cycle diagram reproduced in Fig. 9. Based upon a unit weight of 1 kg. of air, with L_1, L_2, L_3, and L_4 expressed in terms of heat, it is:

$$L_1 = C_v (T_2 - T_1); \quad T_2 = T_1 \left(\frac{p_2}{p_1}\right)^{\frac{n-1}{n}}$$

and therefore

$$L_1 = C_v T_1 \left(\frac{p_2}{p_1}\right)^{\frac{n-1}{n}} - 1$$

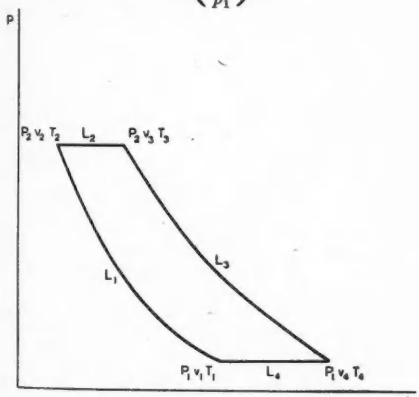

Fig. 9. **Cycle diagram of jet propulsion process.**

If q denotes the amount of fuel in kg. admitted per second, and I its calorific value in kcal./kg., it is

$$q \cdot I = C_p (T_3 - T_2)$$

Therefore:

$$T_3 = T_1 \left(\frac{p_2}{p_1}\right)^{\frac{n-1}{n}} + \frac{q \cdot I}{C_p},$$

and

$$L_2 = A \cdot R \ (T_3 - T_2)$$

Hence it is

$$L_2 = \frac{A \cdot R \cdot q \cdot I}{C_p} \text{ kcal./kg.}$$

It is

$$L_3 = C_v (T_3 - T_4),$$

where

$$T_4 = T_3 \left(\frac{p_1}{p_2}\right)^{\frac{n-1}{n}}$$

Therefore

$$L_3 = C_v \left[T_1 \left(\frac{p_2}{p_1}\right)^{\frac{n-1}{n}} + \frac{q \cdot I}{C_p}\right]\left[1 - \left(\frac{p_1}{p_2}\right)^{\frac{n-1}{n}}\right] \text{ kcal./kg.}$$

and

$$L_4 = A R (T_4 - T_1)$$

$$= A \cdot R \cdot \left[\left[T_1 \left(\frac{p_2}{p_1}\right)^{\frac{n-1}{n}} + \frac{q \cdot I \cdot}{C_p}\right] \times \times \left(\frac{p_1}{p_2}\right)^{\frac{n-1}{n}} - T_1\right]$$

Making $\left(\frac{p_2}{p_1}\right)^{\frac{n-1}{n}} = \epsilon$ and $\frac{q \cdot I}{C_p} = a$,

the output obtained per kg. of air per second is given by

$$N_t = (T_1 \epsilon + a)\left(C_v - \left(\frac{C_v}{\epsilon} - \frac{A R}{\epsilon}\right) - C_v T_1 \ (\epsilon - 1) + AR (a + T_1)\right)$$

The thermal efficiency is given by $\eta_t = \frac{N_t}{qI}$, or

$\eta_t = 1 - \frac{T_4}{T_3}$, or also $\eta_t = 1 - \left(\frac{p_1}{p_2}\right)^{\frac{n-1}{n}}$.

The latter relationship is charted in Fig. 10.

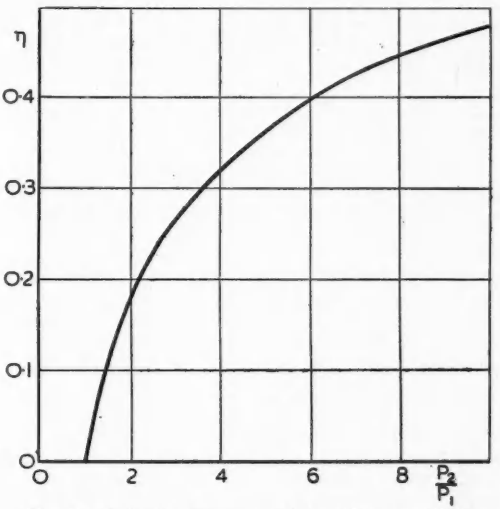

Fig. 10. **Influence of compression ratio upon efficiency.**

The efficiency is thus seen to be a function of the compression ratio. In fact, this relationship is identical with that existing in the case of the internal combustion engine. It must, however, be noted that because of the large volume of air involved in jet propulsion, the combustion chamber of a jet propulsion plant cannot be designed for very high pressure lest its weight would become excessive.

If N_t represents the energy expended upon increasing the gas velocity from v to w (m./sec.), and if η_d denotes

the efficiency of the jet nozzle, it is

$$\frac{w^2}{2g} - \frac{v^2}{2g} = \frac{\eta_d N_t}{A}$$

and

$$w = \sqrt{\left(\frac{2g\eta_d}{A}\right) \cdot N_t + v^2}$$

The propulsive force P is

$$P = m\left[\sqrt{\frac{2g\,\eta_d}{A}\left[(T_1\epsilon + a)\left(C_v - \frac{C_v}{\epsilon} - \frac{AR}{\epsilon}\right) - C_v T_1(\epsilon - 1) + AR(a + T_1)\right] + v^2} - v\right]$$

and the efficiency

$$\eta = \frac{1}{2v}\left[\sqrt{\frac{2g \cdot \eta_d}{A}\left[(T_1\epsilon + a)\left(C_v - \frac{C_v}{\epsilon} - \frac{AR}{\epsilon}\right) - C_v T_1(\epsilon - 1) + AR(a + T_1)\right] + v^2} + v\right]$$

These expressions are, however, purely theoretical, and in actual cases the efficiency of the compressor and its drive must be taken into account.

Aerodynamic aspects.

At the maximum velocity which the jet driven plane can attain, the propelling force will equal the air resistance. The latter is given by

$$W = C_w \cdot \frac{\gamma \cdot v^2}{2 \cdot g} F,$$

where C_w is the drag coefficient and F is the wing area.

Making $C_w\,\gamma\,\frac{F}{2 \cdot g} = k$ it becomes

$$m(w - v) = k \cdot v^2$$

or

$$v = -\frac{m}{2k} + \sqrt{\frac{m^2}{4k^2} + \frac{m \cdot w}{k}}$$

Highest top speed is therefore conditional upon a small value for k, and an inherently small wing area, a small value for C_w, a high gas velocity w, and a large value for m (that is to say, a large gas discharge per second); a small value for γ, that is, high altitude, is also required. With respect to the latter, the decrease in the value for m with the altitude constitutes, however, a limiting factor.

From the expression given for v it is seen that a relatively large increase in the gas velocity w must be effected if a considerable increase in the speed v of the aircraft is to be obtained. But this requirement leads to low volumes for $\frac{v}{w}$. The efficiency must therefore remain quite low. Nor is it feasible to increase the mass of gas ejected per second above a certain limit, since this would call for an unduly large propulsion plant. The operating economy of the jet propulsion plant will therefore be low and the use of jet propulsion will have to be restricted to cases where highest speed requirements override economic considerations.

THE STRUCTURE OF HARD METAL ALLOYS.

By W. Dawiml and J. Hinüber. (From *Kolloid Zeitschrift*, Vol. 104, August/September, 1943, pp. 233-236.)

Two primary characteristics are mainly responsible for the outstanding abrasion resistance properties of hard metal alloys of the tungsten-carbide type with 60 per cent of a low melting metal (cobalt).

(1) In practice, hard metal alloys when mechanically stressed undergo elastic deformation only. Even a compressive stress of 400 kg./mm² leaves no permanent deformation after application to a WC + 6 per cent Co alloy.

(2) The abrasive effect of other metallic materials on hard metal alloys is comparatively low. An investigation into the working life of hard-metal cutting tools has shown that with up to about 10 per cent cobalt content, the life of the tool is hardly reduced. With the addition of more cobalt, however, a more rapid decrease in the life of the tool was caused than was expected from the increased cobalt content. At the same time it was observed that tungsten-carbide alloys containing more than 10 per cent cobalt suffered permanent deformation when mechanically stressed.

Leaching experiments, by boiling thin sintered plates in hydrochloric acid, provided a structural explanation for these properties of hard metal alloys.[2] With a cobalt content of less than 10 per cent a strong network of firmly adhering tungsten-carbide crystals is formed. The cobalt is found in the spaces of this network and the properties of the sinter compact will be governed by this structure—so long as the tungsten-carbide network is homogenous throughout the whole compact. The results of the leaching experiments, correlated in Table I, show, however, that an alloy containing 20 per cent cobalt breaks down into small pieces. Such a breakdown appears to be incipient already in the 10 per cent cobalt alloys.

Table 1.
Leaching experiments on sintered metals of tungsten-carbide with varying cobalt content.

Cobalt content of material at outset.	Total leaching time in hours.	Cobalt content of leached material.	Remarks.
Per cent.		Per cent.	
1.0	377	0.04	Plates apparently unchanged.
6.0	377	0.04	Plates apparently unchanged.
10.0	117	0.01	A few cup-shaped pieces have burst from the plates.
20.0	72	0.01	After 20 hours, the plates break down into small cup-shaped pieces.

It may therefore be assumed that, under normal conditions of manufacture, a complete tungsten-carbide network is no longer formed in alloys containing more than about 10 per cent cobalt. This would explain the setting in of permanent deformations and the marked decrease in resistance to wear. The much shorter leaching time required for alloys with a higher cobalt content, also indicates the formation of fairly large self-contained network complexes entirely surrounded by cobalt.

In order to substantiate further to this theory of a continuous tungsten-carbide network, the mechanical strength of hard metal alloy samples was determined after the removal of the cobalt by leaching. Rods 70 mm. long and 6 mm. diameter were used for these tests. The amount of cobalt still contained in the sample rods was determined by assaying the fractured pieces after testing. The values recorded for the mechanical properties in Table 2 are the mean of five determinations.

TABLE 2.
The strength of the tungsten-carbide net work.

Cobalt content before leaching.	Bending strength before leaching.	Bending strength after leaching.	Cobalt content after leaching.
Per cent.	kg./mm.^{2}	kg./mm.^{2}	Per cent.
3.0	126	54	0.04
6.0	165	45	0.04
11.0	182	crumbled	0.03

These strength values indicate that even after leaching, considerable strength is retained in the residual material, and this is of the same order as that of tungsten-carbides sintered without a matrix metal. It has not yet been possible to determine to what extent the residual traces of cobalt are held in solution in the tungsten-carbide net work. But the fact that in a mixture of WC alloy with 6 per cent cobalt, even after sintering at 1000 deg. C. (a temperature at which no shrinkage has yet occurred), leaching experiments have indicated the presence of a continuous tungsten-carbide net work, suggests that the cobalt plays primarily the part of an intermediate substance aiding the growth of the tungsten-carbide crystals into an interlocking net work.

The degree of completeness of the net work formed depends also, apart from the increasing cobalt content, on a series of other factors such as grain size of the tungsten-carbide and conditions of manufacture and sintering. The leaching experiments, as well as past experience, have indicated the influence of these additional factors. A gradual transition from a complete tungsten-carbide network to complete solution of the network in the cobalt matrix, with increasing cobalt content, may therefore be expected. This is indicated also by dilatometric measurements on hard-metal rods of tungsten-carbide with varying cobalt content. The diagramatic representation Fig. 1 shows that up to about 10 per cent cobalt, the coefficient expansion alters but little with increasing cobalt content. Thus it appears, that the expansion is mainly that due to the tungsten-carbide network, although it may be assumed that owing to the slight increase, a certain compressive effect, i.e., an elastic strain of the network, is set up by virtue of the greater coefficient of expansion. Above 10 per cent cobalt the coefficient of expansion of the mixture gradually increases and the curve slowly approaches the straight line relationship which would hold if the coefficient of expansion were equal to the cumulative expansions of the constituents.

There appears to be no sharp kink in the curve to indicate the sudden solution of the network in the matrix at some well-defined composition. It is of importance to note that no influence of porosity on the coefficient of expansion could be observed within the limits of accuracy of the measurements.

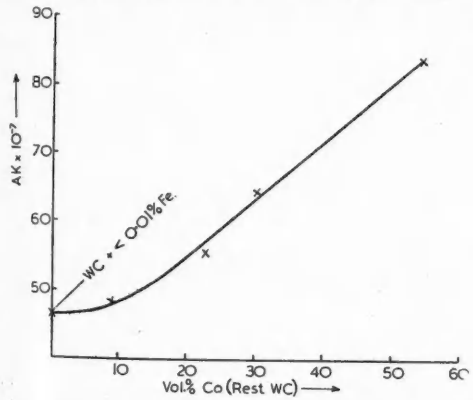

Fig. 1. **Expansion of sintered mixture of WC and Co.**

The fact that the critical alloy composition for the suppression of network formation can be displayed by alteration of the sintering conditions, adds strength to the view that the conditions required for the growth of the net work do not change suddenly. Thus an alloy containing 11 per cent cobalt sintered normally, i.e., for approximately 1 hour, crumbles when the cobalt has been leached out. After sintering for 120 hours, however, the alloy retains a critical bending moment of 18.6 kg./mm^2 after similar leaching treatment. During prolonged sintering, partial net work formation is undoubtedly caused by the production of points of contact between tungsten-carbide grains originally separated by the matrix metal. Thus, the marked grain growth caused by re-crystallisation plays its part in the formation of the tungsten carbide network under these conditions. This phenomenon is well illustrated by Fig. 2.

Fig. 2. **Structure of WC + 11 per cent Co sintered 120 hours at 1450 deg. C. Cobalt leached with Hcl (magn. × 1500).**

When the strength of the leach-treaated sinter compact is evaluated, due consideration must be taken of the fact that at a sintering temperature of 1400 deg. C the cobalt contains approximately 10 per cent WC in solid solution. This means that removal of the cobalt causes an appreciable voidage formation as shown below.

Co content of the WC alloy.	Voidage after leaching.
Per cent.	Per cent.
3	6.1
6	12
11	22

In practice the voidage is much greater owing to the porosity of the untreated compact and incompleteness of the net work structure.

In Fig. 3 the effect of sintering temperature on the critical bending moment of pure tungsten-carbide is shown. Similar curves for alloy G1 (6 per cent Co) and alloy G2 (11 per cent Co) are plotted for comparison. These curves indicate that the addition of cobalt, by virtue of its properties in aiding the sintering process, reduces the sintering temperature required for optimum bending strength from 1800 deg. C for pure WC to 1300 deg. C for alloy G2.

The sudden reduction in strength of alloy G2 at sintering temperatures above 1600 deg. C is explained by the fact that increased diffusion and solution processes cause a marked change in the lattice structure of alloy which undergoes an increase in volume. This is clearly shown in Fig. 4 where changes in the diameter of the sample are plotted against the sintering tempera-

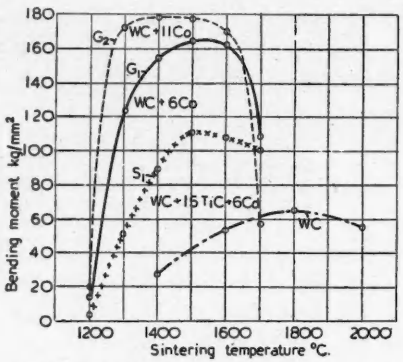

Fig. 3. **The relationship between sintering temperature and bending moment for WC, G_1, G_2 and S_1.**

ture. The addition of titanium carbide to the straight tungsten carbide-cobalt alloys raises the temperature required to achieve the greatest strength of the alloy. (See alloy S1, WC 15 per cent TiC 6 per cent Co). It can also have been seen that the temperature range for satisfactory sintering of multi-carbide alloys is considerably more critical than for straight tungsten carbide-cobalt alloys. It is noteworthy that the sintering temperature of a carbide can only be lowered by those metals which are able to undergo a solution process. Insoluble metals, such as copper, inhibit the sintering process, and thus raise the sintering temperature required for the attainment of optimum strength.

CONCLUSION.—Determination of the strength of the

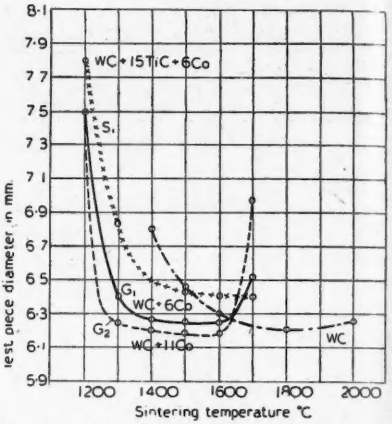

Fig. 4. **Relationship between sintering temperature and the diameter of test pieces of WC and alloys G_1, G_2 and S_1.**

carbide network gave further confirmation to the theory that the formation of a tungsten-carbide network is the reason for the great rigidity of these hard-metal alloys and is therefore the cause of their great hardness and resistance to abrasion. The theory of the network structure of hard-metal alloys is further supported by measurements of expansion and strength in relation to cobalt content and determinations of structure.

REFERENCES.

(1) W. Dawihl, Z. techn. Physik 21,336 (1940).
(2) W. Dawihl, Stahl u. Eisen 61,210 (1941).

A NOVEL AUTOMATIC SYNCHRONIZER

(See *The Engineers' Digest*, Vol. VI, No. 5, pp. 136/137)

THE synchronizing device described in our last issue has proved of special interest to our readers. The following additions may, therefore, be made: The accuracy of the instrument is evidenced by the oscillograms reproduced in Figs. 4a and 4b.

In this case the time lag of the main switch is 0.5 sec., the beats being 13 and 2 seconds respectively. The ability of the synchronizing device to operate under extreme conditions is illustrated by the oscillograms given in Figs. 5*a* and 5*b*. In the case of Fig. 5*a*, the beat is seen to be only 0.48 seconds, corresponding to an extremely large frequency difference of 4.2 per cent, while the oscillogram, Fig. 5*b*, was taken with the use of a main switch having the extremely long closing time of 0.8 seconds.

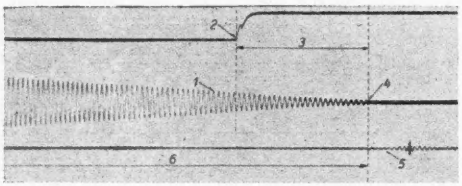

Fig. 4*a*.—(6) Beat: 13 sec. = 0.15 per cent frequency differential
(5) Equalising current I = 0.1 In.
(3) Closing time of switch: 0.5 sec.

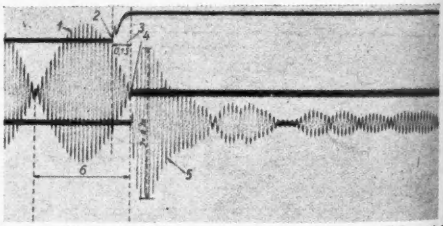

Fig. 5*a*.—(6) Beat: 0.48 sec. = 4.2 per cent frequency differential.
(5) Equalising current I = 2 In.
(3) Closing time of switch: 0.1 sec.

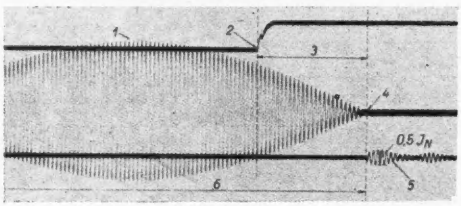

Fig. 4*b*.—(6) Beat: 2 sec. = 1.0 per cent frequency differential.
(3) Closing time of switch: 0.5 sec.
(5) Equalising current I. = 0.5 In.

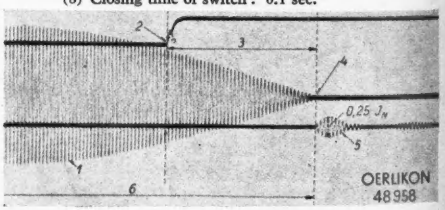

Fig. 5*b*.—(6) Beat: 3.3 sec. = 0.6 per cent frequency differential.
(5) Equalising curent I. = 0.2 In.
(3) Closing time of switch: 0.8 sec.

Figs. 4 and 5. **Oscillograms showing operation of synchronizer.**

and the
.
to the
etwork
l-metal
ardness
etwork
ted by
tion to

ograms
5*a*, the
ing to
r cent,
he use
g time

erential.

ON
8

erential.